Materials Today Energy 31 (2023) 101229

Contents lists available at ScienceDirect

Materials Today Energy

journal homepage: www.journals.elsevier.com/materials-today-energy/

Toward high efficiency at high temperatures: Recent progress and prospects on InGaN-Based solar cells

Yuji Zhao [a, b, *], Mingfei Xu [a], Xuanqi Huang [b], Justin Lebeau [c], Tao Li [a], Dawei Wang [b], Houqiang Fu [b], Kai Fu [a, b], Xinqiang Wang [d], Jingyu Lin [e], Hongxing Jiang [e]

[a] Department of Electrical and Computer Engineering, Rice University, Houston, TX, 77005, USA
[b] School of Electrical, Computer and Energy Engineering, Arizona State University, Tempe, AZ, 85287, USA
[c] Department of Materials Science and Nanoengineering, Rice University, Houston, TX, 77005, USA
[d] State Key Laboratory of Artificial Microstructure and Mesoscopic Physics, School of Physics, Peking University, Beijing, 100871, China
[e] Department of Electrical and Computer Engineering, Texas Tech University, Lubbock, TX, 79409, USA

ARTICLE INFO

Article history:
Received 6 September 2022
Received in revised form
8 December 2022
Accepted 9 December 2022
Available online 17 December 2022

Keywords:
InGaN-based solar cells
Epitaxy growth
Device engineering
High temperature performance

ABSTRACT

III-nitride InGaN material is an ideal candidate for the fabrication of high performance photovoltaic (PV) solar cells, especially for high-temperature applications. Over the past decade, significant efforts have been made to improve the PV performance of InGaN-based solar cells. In this paper, we perform a comprehensive review of the recent developments in InGaN-based solar cells. The topics of discussion include theoretical modeling, material epitaxy, device engineering, and high-temperature measurement. Particularly, we highlight subjects such as substrate technology, and properties that are unique to InGaN materials such as polarization control and their positive thermal coefficient. To date, outstanding high-temperature InGaN-based solar cells with quantum efficiency approaching 80% at 450 °C have been demonstrated. Future innovations in epitaxy science, device engineering, and integration methods are required to further advance the efficiency and expand the applications of InGaN-based solar cells.

1. Introduction

Since the 1990s, GaN-based III-nitride semiconductors have aided in the development of high-performance optoelectronic devices, e.g., light-emitting diodes (LEDs) [1,2], laser diodes [3,4], and electronic devices including RF transistors [5,6] and power devices [7,8]. In 2002, it was discovered that InN has a bandgap energy of 0.64 eV, which was much lower than the previously accepted value of 1.9 eV [9]. This new finding expanded the tunable direct bandgap of InGaN materials from ultraviolet (GaN ~3.42 eV) to near infrared (InN ~0.64 eV) spectral regions, providing a near perfect match to the entire air-mass-1.5 solar spectrum [9,10]. InGaN materials also exhibit many other attractive properties, including a large absorption coefficient (10^5 cm^{-1}), high saturation velocities, high mobilities, high thermal stability, and outstanding radiation resistance [9–14]. All of these advantageous features make InGaN materials the ideal candidates for PV applications, especially for high-temperature operation and operations in harsh environments. This includes photovoltaic thermal (PVT) hybrid solar collector systems [15], terrestrial concentrated PV systems [16], and space explorations [17].

Over the last two decades, research efforts on InGaN-based solar cells have increased significantly. First generation InGaN-based solar cells were fabricated on p-i-n structures with thick InGaN layers grown on *c*-plane sapphire substrates. In 2007, Jani et al. [18] reported the first PV response from an InGaN/GaN p-i-n double heterostructure (DH) solar cell with a 200 nm InGaN active layer. This device showed an open circuit voltage (V_{oc}) of 2.4 V and an internal quantum efficiency (IQE) of 60%. Later, Neufeld et al. [19] reported improved device performance from a similar p-i-n DH device with a peak external quantum efficiency (EQE) of 63%, a fill factor (FF) of 75%, a short circuit current density (J_{sc}) of 4.2 mA/cm^2, and a V_{oc} of 1.81 V under concentrated AM0 illumination. In 2009, Horng et al. reported InGaN/GaN solar cells with a bulk InGaN layer of 150 nm, realizing a power conversion efficiency (PCE) of 0.8% [20]. In 2010, Dahal et al. achieved a PCE of 2.95% with an InGaN/GaN multiple quantum well (MQW) structure [21]. It was found that the performance of InGaN-based solar cell devices could be further improved by utilizing strained InGaN/GaN MQWs or superlattice active layer structures, which are similar to the

* Corresponding author. Department of Electrical and Computer Engineering, Rice University, Houston, TX, 77005, USA
E-mail address: yuji.zhao@rice.edu (Y. Zhao).

https://doi.org/10.1016/j.mtener.2022.101229
2468-6069/

structures of commercial LEDs [21–23]. It was argued that these thin QW layers could successfully mitigate the defect issues found in thick InGaN layer structures and therefore lead to improved device performance [16,22,23]. In 2017, Liu et al. demonstrated InGaN/GaN solar cells with an optimized MQW design, which improved the PCE to 3.56% [24]. However, these QW InGaN-based solar cells were commonly grown on polar *c*-plane GaN, which suffers from notorious polarization-related effects [25,26]. It was reported that these effects prohibit the transport of photogenerated carriers in InGaN QWs, thus fundamentally limiting the carrier collection and PCE of InGaN-based solar cells [27,28]. Recently, Huang et al. demonstrated "polarization-free" InGaN/GaN QW solar cells grown on novel nonpolar and semipolar bulk GaN substrates [29–31]. These new solar cells showed significantly improved carrier collection and a high potential to break the PCE limit in current polar devices. Nonetheless, the PCE of current InGaN-based solar cells still lags far behind theoretical values (>20%) [27,32]. The poor PCE can be attributed to low-quality InGaN layers, which suffer from issues such as phase separation, defect generation, polarization effect, and p-type doping. In addition, the thermal performance of InGaN-based solar cells also attracted significant interest [12,13,33–35]. Various groups reported a positive thermal power coefficient for InGaN-based solar cell devices, which is very different from conventional Si or III-V PV devices [12,13]. For example, Huang et al. [30] reported a large working temperature range, from room temperature to 450 °C, for nonpolar InGaN-based solar cells. In addition, these solar cells had positive temperature coefficients for temperatures up to 350 °C. This unique feature indicated that InGaN-based solar cells could potentially be used as the high energy cell in multijunction (MJ) devices for concentrator PV applications, PVT systems, and in space applications where high temperature PV operation is critical.

In this paper, we perform a comprehensive review on the recent development of InGaN-based solar cells, covering key research topics on theoretical simulation, material epitaxy, device engineering, and high-temperature measurement, as summarized in Fig. 1. Following this introduction section, Section 2 discusses the theoretical analysis of InGaN-based solar cells using both house-developed models and commercial software, highlighting the unique impacts from polarizations of III-nitrides. Section 3 presents the material epitaxial growth of InGaN-based solar cells, where recent results on epitaxy methods (e.g., MOCVD vs. MBE), epilayer structures (e.g., bulk materials vs. QWs), and substrate materials (e.g., sapphire substrates vs. bulk GaN substates) will be discussed. Section 4 summarizes the device engineering approaches of InGaN-based solar cells, including polarization control, energy band engineering, and optical design. Section 5 reviews the high-temperature performance of InGaN-based solar cells, including thermal stress performance, positive temperature coefficient, and carrier dynamics at high temperatures. Finally, Section 6 concludes the paper and discusses necessary future work for InGaN-based solar cells to reach their full potential.

2. Theoretical studies

Three major theoretical approaches have been used to study the electronic and optical properties of InGaN-based solar cells: in-house models [43–53], commercial software [27,28,32,36,54–63], and open-source software [64,65].

2.1. In-house models

In-house models of InGaN-based solar cells were largely developed using the classical drift-diffusion model, which was widely used to study Si and III-V solar cells. Key material parameters, such as the bandgap energy and absorption coefficients, were modified to apply the model to the simulation of InGaN-based solar cells. The majority of these works, however, do not consider the polarization effects unique to III-nitride materials. Nevertheless, these early theoretical works provided useful information on the design of InGaN-based solar cells.

For single junction cells, early simulation work was focused on the impacts of material quality and device structures on the performance of InGaN-based solar cells. For example, Feng et al. [45] found that the indium content, thickness, and defect density of the InGaN i-layer had strong effects on the device characteristics of the InGaN-based solar cells. This included the absorption, PCE, J_{sc}, V_{oc}, and PCE of the devices. As expected, increasing indium content in the active region causes absorption and J_{sc} to increase, while V_{oc} and conPCEare reduced, as shown in Fig. 2(a and b). However, authors have underestimated the defect density in the InGaN layers and the effect of these defects on the related material properties. In addition, the degradation of InGaN layers becomes much more severe when more indium is incorporated during growth.

For more advanced structures, Cavassilas et al. [47] theoretically analyzed the PV performance of InGaN-based solar cells with thick InGaN layers and QW structures. They found that a MQW structure balances the trade-off between photon-absorption and electronic transport, which are rival phenomena in nanostructure based solar cells. However, such nanostructures need to be properly designed since the PCE is strongly impacted if the confinement and bias are not carefully controlled.

Recently, Huang et al. [49] analyzed the major loss mechanisms in InGaN-based solar cells using a semi-analytical model. This included transmission loss, thermalization loss, spatial relaxation loss, and recombination loss. Among all of these loss mechanisms, the transmission loss plays the primary role in InGaN-based solar cells due to the large bandgaps of III-nitride materials. In addition, they found Shockley-Read-Hall recombination loss is the dominant recombination process. They also discovered that the optical properties of InGaN layers are mainly determined by the Urbach energy, which has significant impacts on the electrical performance of the solar cells, especially in J_{sc} and V_{oc}.

For tandem solar cells, research efforts were mainly focused on exploring the possibility of integrating III-nitride solar cells with existing devices on Si or III-V. For example, Hsu et al. studied the characteristics of monolithic InGaN/Si two-junction (2J) series-connected solar cells using the air mass 1.5 global irradiance spectrum [44]. This theoretical analysis revealed that the alignment of the Si valence band with the $In_{0.46}Ga_{0.54}N$ conduction band eliminates the need for heavy doping at the InGaN/Si heterointerface. The overall PCE of the two-junction InGaN/Si solar cells can reach more than 31%, and it can be higher than 36% in 500 suns and AM1.5G condition.

Later, Toledo et al. performed a comprehensive theoretical study to investigate the design space of integrated III-nitride/non-III-nitride tandem solar cells [43]. The paper pointed out that an InGaN top cell bonded to a 3J or 4J subcell is the most feasible and practical design. Moreover, the actual device parameter requirements largely depend on the bandgap combinations of the III-nitride top cell and the non-III-nitride subcell. For example, as shown in Fig. 2(c and d), the EQE values of various InGaN top cells are decided by the bandgap combinations.

Furthermore, Huang et al. [49] found that the stringent current matching requirements would lead to a limited choice in the top-junction bandgap for 2J InGaN-based solar cells. A stable and high PCE of 43.5% can be potentially achieved with a limited top-junction bandgap window from 1.70 eV to 1.78 eV. In addition, increasing solar irradiance also boosts the performance of 2J InGaN-based solar cells.

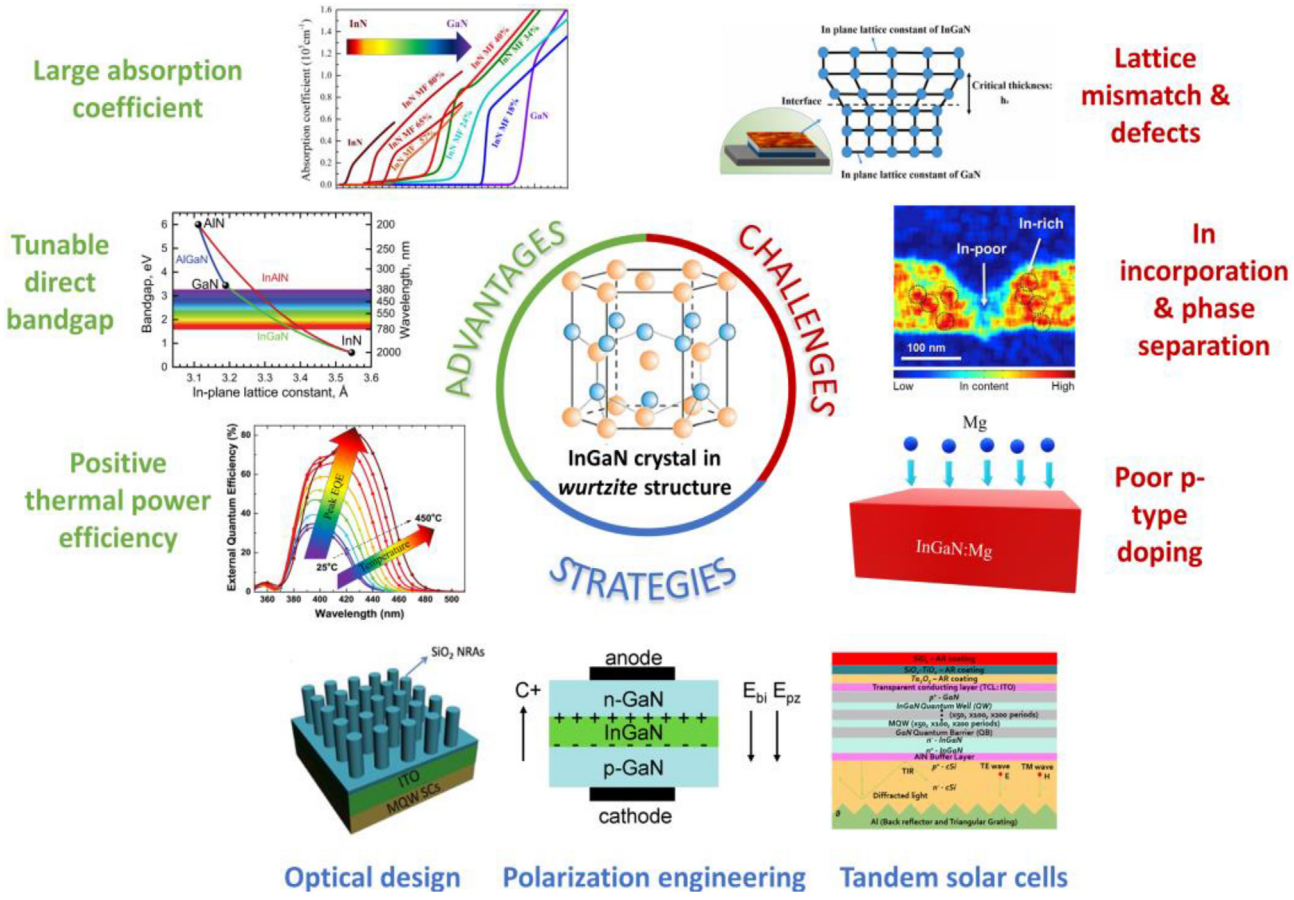

Fig. 1. Advantages, challenges, and strategies of InGaN-based solar cells [30,36–42]. Reprinted with permission from Ref. [30,36,38,41]. Copyright 2018, AIP Publishing. Copyright 2012, Elsevier. Copyright 2021, Elsevier.

2.2. Commercial software and open software

Several companies offer commercial software for solar cell simulations, including APSYS from Crosslight [27,28,32,36,56,57,59,60], Silvaco Atlas [58,62,63], COMSOL [55] and SCSim from STR [61]. Compared with in-house models, these software packages offer more complicated and comprehensive simulations, allowing more accurate materials parameters to be applied.

APSYS is the most widely used solar cell simulator that solves Poisson and drift-diffusion equations self-consistently. Using APSYS, Fabien et al. [28] performed a comprehensive simulation of InGaN-based solar cells with realistic materials parameters, including appropriate p-type doping, background doping, and InGaN layer thickness and indium concentration. They found that the maximum PCE of a p-i-n InGaN/GaN heterojunction solar cell with low indium composition is around 11%, but the PCE reduces drastically for devices with higher indium contents due to strong polarization effects. The paper pointed out that the detrimental polarization effects can be eliminated by using InGaN p-i-n homojunction devices. However, these devices are still far from being feasible. In addition, their simulations also show that the optimal bandgap energy for the solar cells decreases as the background doping increases.

Silvaco Atlas is a commercial device simulation tool based on the drift-diffusion model. It can simulate photovoltaic device performance, including effects such as tunneling and thermionic emission. It can also simulate heterojunction interfaces and full optical models. Fang et al. [62] used this TCAD-based tool to study MQW InGaN-based solar cells at high temperatures and high solar concentrations. These simulation results were compared with experimental data. Their study revealed that polarization effects in InGaN-based solar cells led to a drop in IQE of the solar cells, indicating that polarization reduces the carrier collection efficiency.

In addition, open software has been used for the simulation of InGaN-based solar cells. For example, Jeng et al. [64] used the open software AMPS-1D to simulate the characteristics of InGaN MQW solar cells. However, only energy band diagrams were simulated in their study, possibly due to the limitation of the simulation capability of the software.

These simulation results can provide helpful design guidelines for high-performance InGaN-based solar cells. Instead of using ideal material parameters and simplistic models, more realistic and complex simulation work should be performed. These simulations should consider effects such as defects, doping, and polarization. In addition, the influence of high temperature and high irradiance on the material quality, carrier dynamics, polarization, and performance of InGaN-based solar cells should be a key focus of simulation studies. Moreover, novel solar cell structures such as multijunction solar cells, graded InGaN layers, lattice-matched substrates, and nanostructures should be proposed and simulated to help further increase the PCE of InGaN-based solar cells. As for software choices, AMPS-1D uses Poisson's equation and continuity equations to analyze the transport behavior of 1D structures including homojunction, heterojunction, and multi-junction solar cells. Since it uses a 1D approach, it may not be suitable for realistic 3D structures with

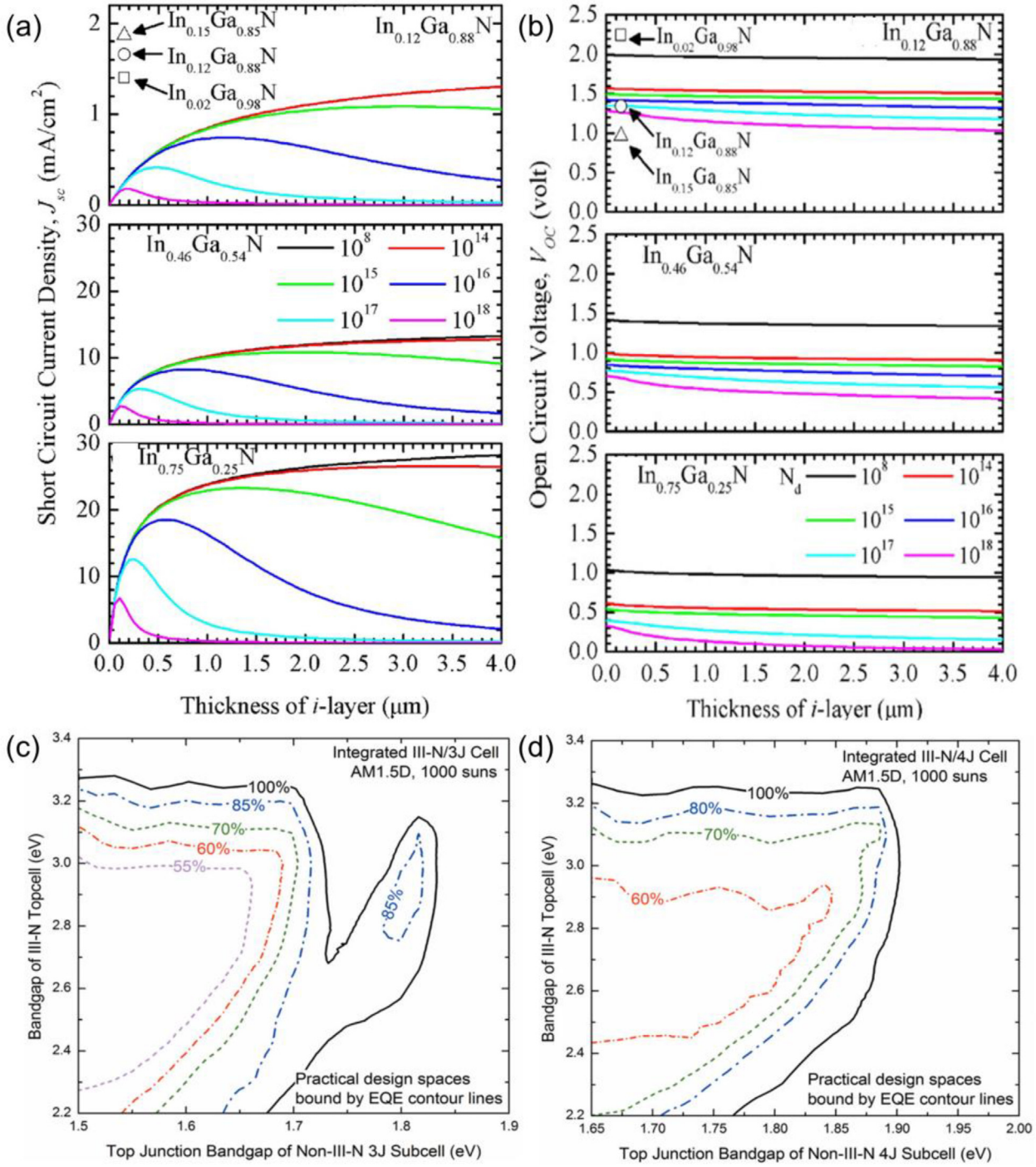

Fig. 2. Simulation of the relationships between InGaN-based solar cell performance and bandgaps/compositions. (a) J_{sc} and (b) V_{oc} as a function of thickness for InGaN-based solar cells with different composition and defect densities. □, ○, and △ denote $In_{0.02}Ga_{0.98}N$, $In_{0.12}Ga_{0.88}N$, and $In_{0.15}Ga_{0.85}N$ *p-i-n* homojunction solar cells with *i*-thickness of 150 nm. Reprinted from Ref. [45] with permission. Copyright 2010, AIP Publishing. (c) Contour lines showing the design space for the EQE values of InGaN top solar cells in an (c) integrated III-nitride/non-III-nitride 3-junction solar cell and in an (d) integrated III-nitride/non-III-nitride 4-junction solar cell under AM1.5D, 1000 suns. Reprinted from Ref. [43] with permission. Copyright 2012, AIP Publishing.

nonhomogeneous properties. The applications of this software are further limited because quantum size effects and tunneling are not accounted for in the simulations. As for APSYS, it uses 2D or 3D finite element methods to analyze the properties of semiconductor devices. The APSYS software has the ability to simulate all of the devices that AMPS-1D can do. Furthermore, the APSYS can also handle more complex devices such as transistors and resonant tunneling diodes. This software also has complex physics models available, including the quantum tunneling and transport model, thermionic emission model, and Poole–Frenkel model. The Silvaco Atlas software provides a series of simulators such as Luminous and S-Pisces for optoelectronic devices. This allows 2D and 3D devices, device operation, and physics models to be simulated, providing a complete analysis for solar cells.

3. Epitaxy growth

3.1. MOCVD vs. MBE

In terms of growth techniques, MOCVD and MBE are the two major methods that are widely used by researchers for the epitaxy of InGaN-based solar cells. There are also limited reports of using a sputtering method to grow InGaN materials for PV applications. InGaN growth using MOCVD has been extensively developed for InGaN LEDs in the ultraviolet to green spectral range. The MOCVD growth method is capable of mass-production of InGaN with a fast growth rate, high throughput, and potential for multi-wafer growth. In comparison, MBE growth of InGaN materials is often used by academic institutes or industrial research laboratories due to the high precision control in layer thickness and interfaces it provides. Drawbacks of this method include its low growth rate and low throughput. Both MBE and MOCVD can produce InGaN layers with indium compositions ranging from 0% to 100%, which is desirable for narrow bandgap InGaN-based solar cells and multi-junction solar cells. Two recent reviews have summarized the growth of InGaN layers by MBE and MOCVD [66,67].

Islam et al. [68] studied the MOCVD growth of InGaN layers for solar cell applications with indium compositions up to 40%. There are two critical parameters used to control the indium composition. The first is trimethylindium/(trimethylindium + triethylgallium) (TMI/(TMI + TEG)) molar ratio or TMI flow rate and the second is growth temperature. Generally speaking, higher TMI flow and lower growth temperature lead to higher indium compositions. They conducted a series of experiments to investigate the effect of TMI flow rate and growth temperatures on InGaN growth. First, the TMI/(TMI + TEG) molar ratio was varied from 0.2 to 0.74 at a growth temperature of 800 °C. When the ratio was 0.2, phase separation was observed due to the instability of InGaN at this ratio [69]. This is because Ga is mostly in the solid phase, while In is in the vapor phase at high temperatures, resulting in inhomogeneity and phase separation. When the ratio was increased to 0.38, the phase separation was suppressed due to the increased supply of In Ref. [70]. Increasing the ratio to 0.74 resulted in not only an increase in indium composition, but also the formation of metallic indium in the InGaN film. The latter is caused by the InN dissociation and indium condensation on the growth surface at a low V/III ratio [71]. The indium formation can be eliminated under a high V/III ratio due to excess nitrogen on the growth surface. Furthermore, they also varied growth temperature from 750 °C to 850 °C at a TMI/(TMI + TEG) molar ratio of 0.38. High quality InGaN films with an indium composition of up to 40% were achieved without phase separation or metallic indium formation. Fig. 3 shows the indium composition as a function of TMI flow rate and growth temperature. The indium composition in the InGaN films increased linearly with an increasing TMI flow rate below 800 °C. Phase separation occurred at low TMI flow rates below 300 sccm. The indium composition decreased linearly with increasing growth temperatures when the TMI/(TMI + TEG) molar ratio was less than 0.38. It has been reported that InN has a low decomposition temperature of 600 °C [72]. High temperatures can cause the evaporation of InN due to the high volatility of nitrogen over InN. Metallic In is more likely to form at both low growth temperatures below 800 °C and high TMI/(TMI + TEG) molar ratios above 0.38. It is also worth noting that growth rate and InGaN film thickness also play a role in the phase separation [73]. Large InGaN film thickness can exacerbate the phase separation caused by strain relaxation as the solid solubility was significantly reduced for relaxed films due to strain [74]. A high growth rate achieved by increasing III sources can help to suppress phase separation, indicating phase separation can be controlled kinetically. To grow high quality InGaN films, the TMI/(TMI + TMG) ratio and V/III ratio needs to be carefully controlled. A low TMI/(TMI + TMG) ratio will cause In desorption and a high TMI/(TMI + TMG) ratio will cause supersaturation. When In concentration increased, a higher V/III ratio should be used to facilitate the In incorporation and suppress the phase separation [66].

In MBE growth, it is easier to incorporate indium into InGaN films than with MOCVD growth. Like in MOCVD growth, high indium compositions in MBE growth can lead to phase separation due to growth kinetics. This includes InN thermal decomposition and indium surface segregation [75]. To solve these issues, it is important to enhance the diffusion rate of In adatoms on the surface to grow non-phase separated InGaN films with high indium compositions. Clinton et al. provided a comprehensive discussion on metal modulated epitaxy (MME) and N-rich low-temperature MBE growth that can produce InGaN films throughout the miscibility gap [66]. MME periodically shutters the effusive cells for Ga and In where nitrogen is always present (i.e., the growth is continuous). Therefore, the growth mode switches between metal-rich growth and N-rich growth. The former can increase adatom mobility, and the latter can be beneficial for p-type doing [66,76]. GaN was first grown by MME as a baseline because binary compound growth is much easier than ternary compound growth (i.e., InGaN). Fig. 4(a) shows the transitioning between Ga-rich growth and N-rich growth for MME GaN films. The MME uses a combination of low growth temperature and high metal fluxes to avoid the intermediate phase regime. This dramatically reduces the formation of surface pits and produces high-quality films. In addition, GaN films with ultrahigh doping concentrations were also realized by MME [77]. With the assistance of in situ feedback from RHEED, MME growth of UID-GaN, p-GaN, and n-GaN were calibrated with repeatable procedures. To grow high-quality InGaN films by MME, phase separation must be solved. As mentioned above, phase separation is caused by thermal decomposition and indium surface segregation. Thermal decomposition can be mitigated by using a low growth temperature, and indium surface segregation can be suppressed by N-rich growth. However, the two growth conditions also lead to low adatom mobility and thus high surface roughness. On the other hand, metal-rich growth can improve film quality but suffers from indium surface segregation. MME growth is proposed to solve this dilemma. Single-phase InGaN films throughout the miscibility gap have been demonstrated by MME growth [66]. However, MME growth can only produce high-quality InGaN films with In composition less than 20% or more than 60%. MME InGaN films with intermediate In compositions from 20% to 60% suffered from high defect densities. Therefore, advanced nucleation and strain relaxation techniques are needed to reduce defect densities. Fabien et al. [77] employed low-temperature N-rich MBE growth to grow InGaN films with In compositions between 20% and 60%, which can suppress the phase separation of InGaN films, as shown in Fig. 4(b). During the InGaN growth, this method involves opening the metal and plasma shutters and using non-traditionally low substrate temperatures in the range of 360 °C–450 °C. MME and low-temperature N-rich MBE growth can be used independently and selected depending on device applications. MME growth can produce high-quality smooth films with any thickness, GaN films with high doping concentrations, and InGaN films spanning the miscibility gap. However, MME InGaN films with In composition less than 60% have large defect densities and low optical emission. Low-temperature N-rich MBE growth is suitable for growing InGaN films with In compositions between 20% and 60%, which is important for solar cell applications. However, this method is limited to thin InGaN films because the surface roughness increases with increasing film thickness.

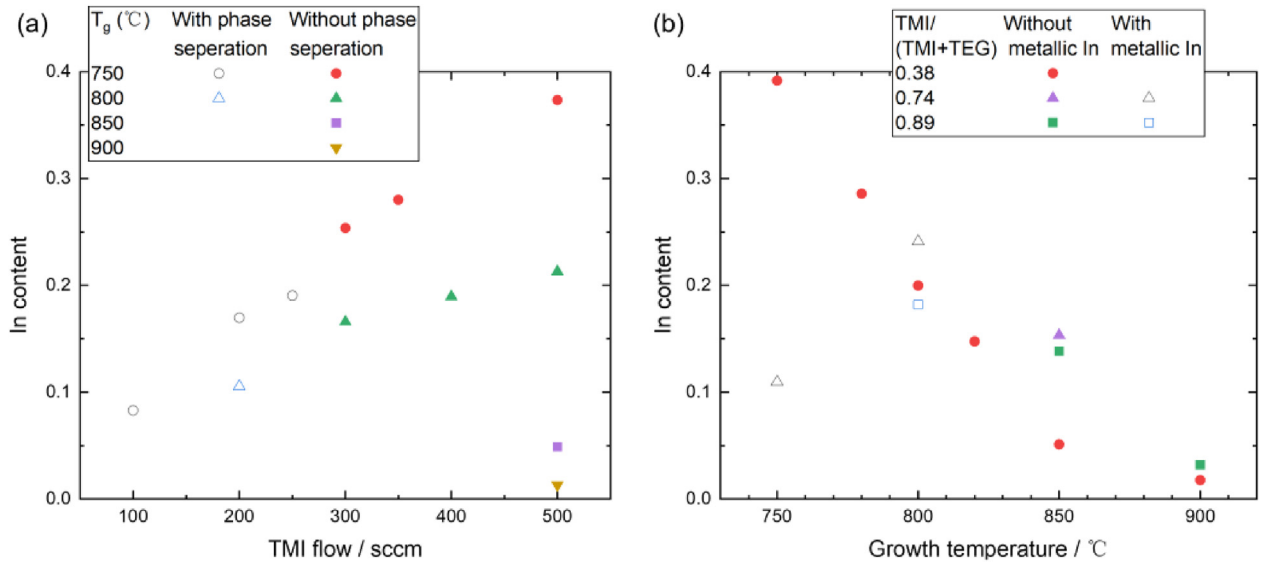

Fig. 3. Quality of InGaN films under different growth conditions (a) In composition as a function of TMI flow rate at different growth temperatures. (b) In composition as a function of growth temperature at different TMI/(TMI + TEG) molar ratios. Reprinted from Ref. [68] with permission. Copyright 2013, Elsevier.

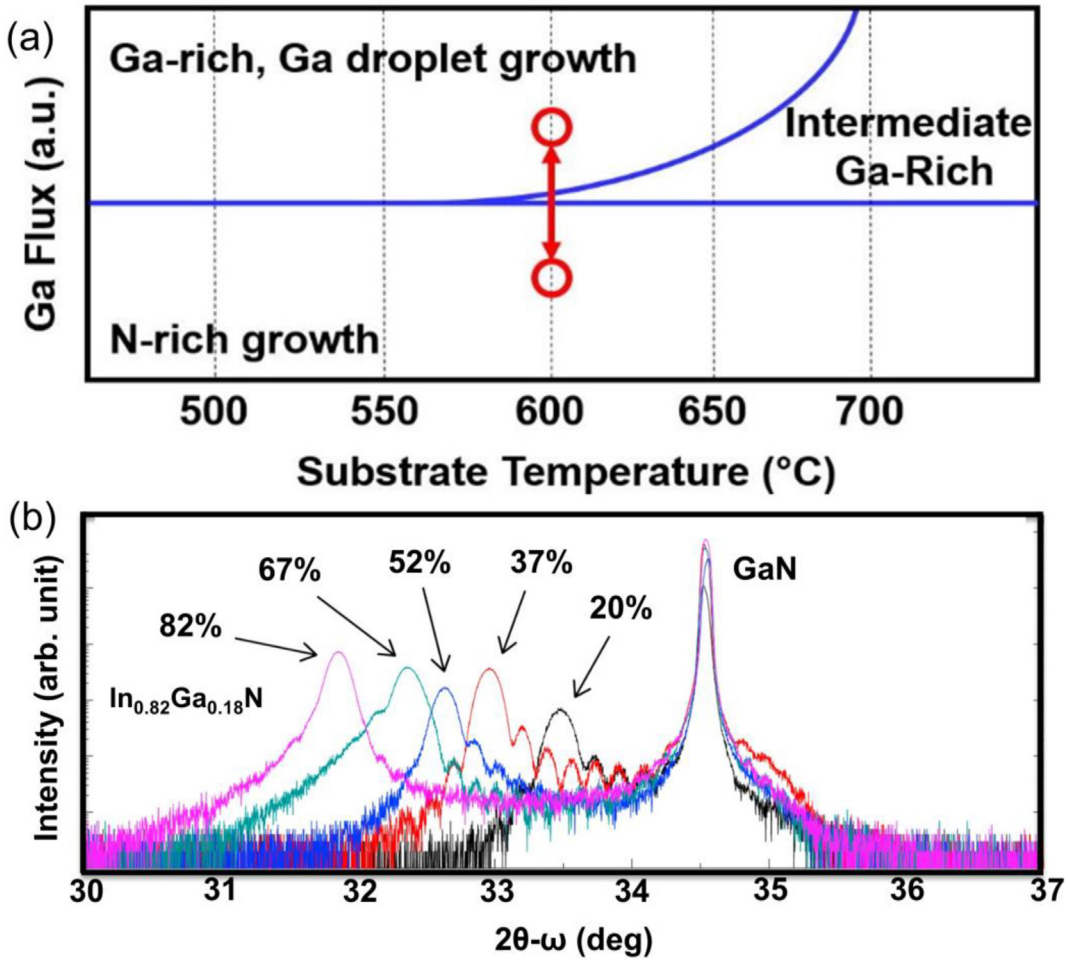

Fig. 4. MME growth for single-phase InGaN films. (a) Growth diagram of GaN by MME. Reprinted from Ref. [66] with permission. Copyright 2017, Elsevier. (b) $2\theta-\omega$ diffraction patterns of InGaN films of different composition. Reprinted from Ref. [77] with permission. Copyright 2015, Elsevier.

3.2. Bulk InGaN vs. QWs

Growth of the InGaN active layer for III-nitride solar cells can be roughly divided into two categories: bulk structure and MQW structure. For Si, III-V and II-IV solar cells, a thick active layer (e.g., bulk structure), is the most common design. This is because these devices usually require an absorber with a thickness larger than 1 μm to fully absorb the incoming light spectrum. However, it is extremely difficult to grow bulk InGaN layers due to previously mentioned challenges, especially with high indium compositions. Furthermore, the use of foreign substrates such as sapphire or Si degrades the material quality of InGaN and results in basal stacking faults and threading dislocations in an order of 10^9–10^{10} cm^{-3} [78]. Early demonstrations of InGaN-based solar cells have been mainly based on bulk InGaN layers with either p-i-n or p-n structures [18–20,79–82]. The common features of cells with bulk InGaN layers are their low V_{oc} and the relatively high J_{sc} values. Typical V_{oc} lower than 2 V as well as large voltage-bandgap offsets (W_{oc}) in such structures can be attributed to the low quality of InGaN absorbers. Fig. 5(a and b) show that the V_{oc} of bulk solar cells drops rapidly with increasing In concentration, while the V_{oc} of MQW solar cells only decreases slightly with In concentration up to 45%. Recent results show that a bulk InGaN layer with a thickness of more than 100 nm can be realized through both MOCVD and MBE approaches. For example, Islam et al. [68] reported the MOCVD growth of InGaN films with an indium fraction up to 39% and a thickness up to 650 nm. However, phase separation and severe strain relaxation were observed in such InGaN films. Several groups have even reported a more than 1000 nm (1 μm) InGaN layer [68,83]. Nonetheless, the PV performance of those devices is still far from satisfactory and below the theoretical limits. For example, the V_{oc} values are particularly lower than 1 V, indicating degraded material quality. This is attributed to the large amounts of defects and dislocations generated during the growth which strongly impact the material quality [66]. Therefore, the two major challenges for InGaN bulk growth are the large lattice mismatch between InGaN alloys and GaN (due to the lack of suitable native substrate) and the limited miscibility of InN and GaN.

Due to these challenges with bulk structure growth, MQW structures have been adopted in the development of InGaN PV devices to better preserve material quality and maintain relatively good device performance. These structures are similar to the InGaN-based LEDs [11–13,21–23,25]. The film quality of InGaN absorbing layers is better maintained in MQWs since each InGaN layer is below critical thickness and is also strained in each QW period. The QWs and QBs should be designed to minimize lattice mismatch and reduce strain. A net strain will cause the relaxation of

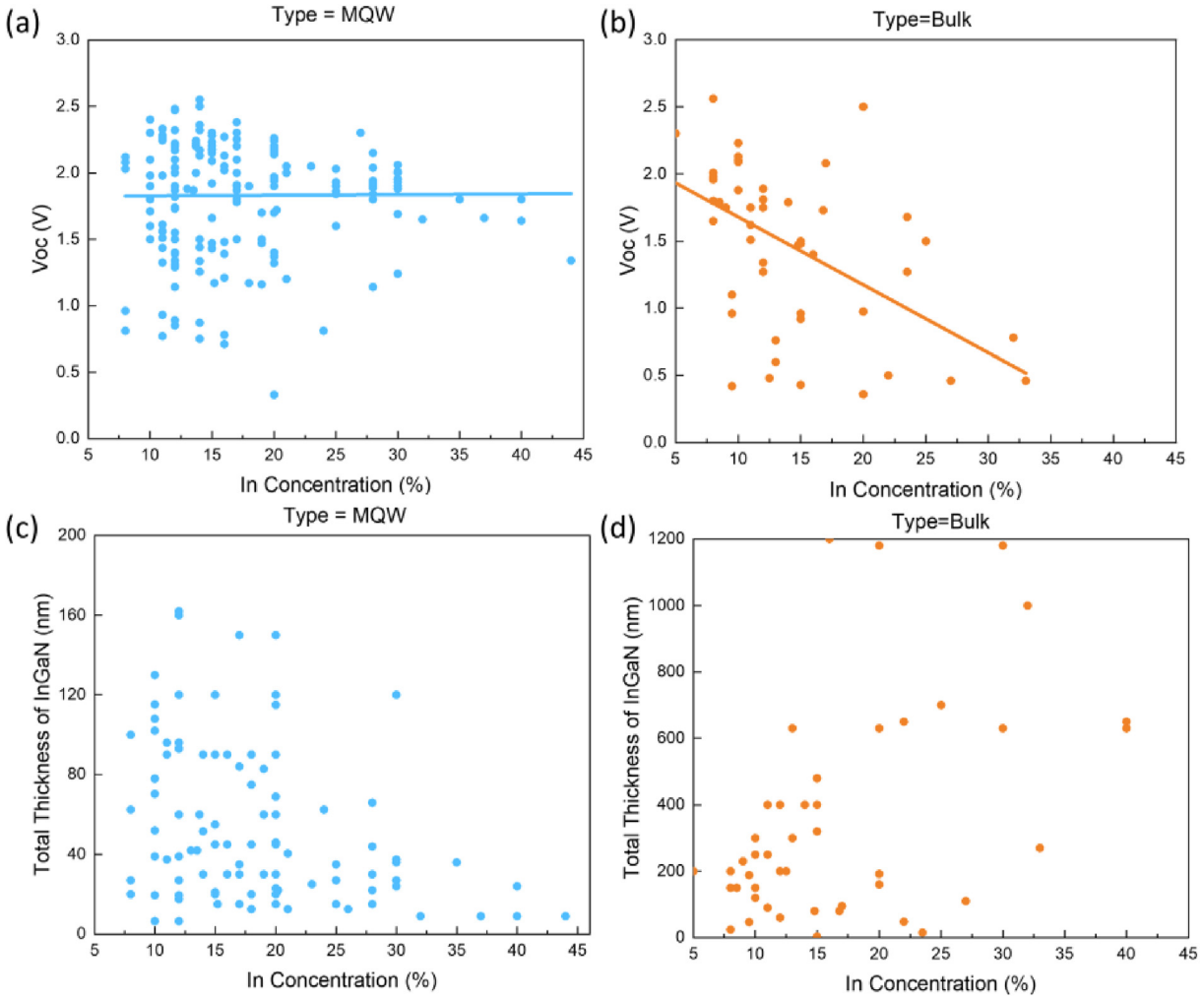

Fig. 5. (a) and (b) V_{oc} of solar cells as a function of indium concentration for MQW structure and bulk, respectively. Solid lines roughly fit the trends between V_{oc} and indium concentration of two structures, (c) and (d) total thickness of InGaN layers as a function of indium concentration for MQW structure and bulk, respectively. Solid dots with different colors represent various substrate choices and different shapes for different growth methods.

layers and generate dislocations. The following equation can serve as a simple guideline to design QWs and QBs [84]:

$$(a_w - a_{temp})t_w = (a_b - a_{temp})t_b$$

where t_w and t_b are the thickness of QWs and QBs, and a_w, a_b, and a_{temp} are the lattice constant of QWs, QBs and, the template.

Since the lattice constant of the QWs depends on In concentration, the thickness of QWs and QBs should be adjusted accordingly to reduce lattice mismatch. InGaN-based solar cells with MQWs or SL generally exhibit V_{oc} values larger than 2 V and small W_{oc} values of around 0.5 V despite having relatively low J_{sc}. As shown in Fig. 5(c and d), the total thickness of InGaN layers with a MQW structure is mostly limited to 100 nm while grown using the MOCVD method. This is related to the thin QW in the MQW structure, which is usually below 6 nm. In this case, if the number of periods of MQW exceeds a certain value, the stress in the epi-layers could induce more defects and threading dislocations, and eventually result in severe structure deterioration [84]. As a result, it is very difficult to increase or even maintain device performance measures such as PCE by increasing the periods of the MQW. Nonetheless, a total thickness of InGaN layers with at least 200 nm is required for the complete absorption of incoming sunlight, which remains a great hurdle even with MQWs or SL structures. Furthermore, there are few reports on InGaN devices with indium compositions larger than 35%. This is attributed to the aggravated indium segregation and phase separation that occurs with more indium in the InGaN layers, which leads to severely degraded material quality and structural integrity.

Several groups and organizations have thoroughly investigated QW structures and their related PV properties, including the periods of QWs [85], the thickness of QWs [86,87], and the thickness of barriers [88–90]. The periods of QWs and the related active region thickness can be tuned to modify the PV performance of MQW solar cells [85]. The EQE of the devices was firstly increased by increasing the periods of QWs, which improved light absorption in thicker active regions. Further increase in the periods, however, only resulted in the saturation of the EQE. Based on calculation and capacitance-voltage measurements, the depletion width was found to saturate with the increase of periods, which left a large region of MQW not depleted and led to the enhanced recombination of carriers in this region. Therefore, it is important to delicately control the active region thickness to enhance the light absorption and fulfill complete depletion.

Redaelli et al. have extensively explored the influence of the thickness of QWs and barriers on the PV performance of solar cells [86,88]. They characterized the properties of solar cells with increasing thickness of QWs. Based on the Cathodoluminescence (CL) measurements, the emission wavelength would redshift with increasing QW thickness due to the decrease in band-to-band transition energy. Meanwhile, the increase in the thickness of QWs would induce the generation of defects by strain relaxation which causes nonradiative recombination. Also, the increase of QW thickness results in decreased overlap of ground state carrier wavefunctions due to the quantum confined Stark effect (QCSE). Similarly, they pointed out that the band-to-band transition energy was enlarged by the reduction of the thickness of barriers resulting in the blueshift of the absorption edge. Moreover, the enhanced carrier wavefunction overlap and the efficient carrier extraction facilitated by the increased tunneling possibility of carriers led to improved EQE and superior performance. In general, the thickness of both QWs and barriers needs to be appropriately tuned to maintain the pseudomorphic growth of MQWs, increase the absorption of the incident light, and prompt the transportation and collection of carriers.

Table 1 summarizes the literature in recent 6 years for InGaN-based solar cells with different structures and growth conditions. Clearly, the development of InGaN-based PV devices will be a great challenge considering the great number of parameters and steps that need to be carefully controlled. It's imperative to optimize the growth condition for InGaN layers with tunable In concentration and proper thickness and develop lattice-matched substrates for the devices. In the meanwhile, nanostructures can be an alternative for the absorber layer design, because they have unique properties compared to thin films and have been widely used in III-nitride growth and InGaN-based optoelectronics [91–96].

3.3. Sapphire substates vs. bulk GaN substates

The choice of substrate materials also plays a vital role in the fabrication of high-quality solar cells. Candidates include sapphire, GaN, strain-relaxed InGaN, Si, and SiC. Sapphire substrates, including patterned sapphire substrate (PSS), are the dominant choices due to their low cost, easy availability, high-temperature stability, and transparent nature [13,18,21,80,83,110–112]. Nonetheless, owing to the large lattice and thermal mismatch between sapphire and GaN, the InGaN films grown on sapphire generate a high density of dislocation defects, which can reduce the quantum efficiency of solar cells [113,114]. To mitigate this problem, GaN buffer layers are usually grown on sapphire before the growth of InGaN layers to diminish the mismatch [115]. Native GaN substrates have also attracted research attention and have been employed for growing InGaN layers as the GaN substrate technology is maturing on the market [29–31,112]. Devices grown on GaN substrates have generally demonstrated better PV performance than their counterparts grown on sapphire [23,112]. Recently, semipolar $(20\bar{2}1)$ and nonpolar m-plane GaN substrates have attracted the interest of researchers [29–31]. Compared to conventional polar c-plane GaN substrates, InGaN-based solar cells grown on the semipolar and nonpolar GaN substrates have reduced polarization, which facilitates carrier collection and leads to better performance. However, even with the reduced defect density of ~10^6 cm^{-3} in the native GaN substrates, the compressive stress in the InGaN layers still needs to be carefully managed to avoid defect generation. In this regard, InGaN templates/substrates could provide better solutions for these issues than GaN substrates [116–118]. Hestroffer et al. reported the growth of a fully relaxed $In_{0.1}Ga_{0.9}N$ layer by plasma-assisted molecular beam epitaxy (PAMBE) [118]. An 800 nm graded InGaN buffer layer with In concentrations ranging from 0 to 18% was first grown by varying the Ga flux, followed by the growth of a 520 nm $In_{0.1}Ga_{0.9}N$ layer. The relaxation was explained by the climb of edge dislocations and dislocation glide. The fully relaxed layer can effectively reduce the lattice mismatch and lower dislocation defect density. Si and SiC substrates are alternative choices for InGaN layer growth [119–121]. Si substrates benefit from low cost, easy availability, and larger thermal conductivity than sapphire. Still, Si substrates suffer from an even larger lattice mismatch with GaN, which hinders their applications. 6H–SiC substrates have a relatively small lattice mismatch with GaN and have a larger thermal conductivity. However, the bulk 6H–SiC substrates are expensive, which makes them unsuitable for commercialization.

4. Device engineering

4.1. Polarization control

Many theoretical simulations and experimental investigations have demonstrated the influence of polarization on III-V nitride materials and devices [30,36,48,56,57,60,65,122–124]. InN and

Table 1
Reports on InGaN-based solar cells.

No.	Structure (Substrate)	InGaN layer (nm) (Growth method)	Peak EQE (%)	Champion PCE (%)	Highlight	Ref.
1	InGaN/GaN MQWs (Sapphire)	$In_{0.1}Ga_{0.9}N$(3.2)/GaN(5.5) 22 periods (MOCVD)	64	1.12	Comparison of AlN and sapphire substrates	[97]
2	GaN/InGaN MQWs (Sapphire)	$In_{0.04}Ga_{0.96}N$(2.5)/GaN(6) 10 periods (MOCVD)	N/A	1.61	Superlattice structure	[98]
3	GaN/InGaN MQWs (Sapphire)	$In_{0.1}Ga_{0.9}N$(3.2)/GaN(3.3) 36 periods (MOCVD)	84	1.31	Effect of QW thickness	[87]
4	p-AlGaN/InGaN/GaN MQWs/n-AlGaN (Sapphire)	$In_{0.1}Ga_{0.9}N$(3)/GaN(7) 30 periods (MOCVD)	57	1.77	AlGaN blocking layers	[54]
5	Ag nanoparticles/InGaN/GaN MQWs (Sapphire)	$In_{0.25}Ga_{0.75}N$(3)/GaN(13) 9 periods (MOCVD)	N/A	0.98	Plasmonic and piezo-phototronic effect	[99]
6	InGaN/GaN MQWs (Sapphire)	$In_{0.25}Ga_{0.75}N$(3)/GaN(13) 9 periods (MOCVD)	N/A	1.24	Piezo-phototronic effect	[100]
7	InGaN/GaN MQWs (Sapphire)	$In_{0.137}Ga_{0.863}N$(3)/GaN(5.6) 20 periods (MOCVD)	36	1.32	GaN tunnel junction contact	[101]
8	InGaN/GaN MQWs (Sapphire)	$In_{0.08}Ga_{0.92}N$(24)/GaN(2) 6 periods (MOCVD)	85	0.39	Semibulk absorber	[102]
9	InGaN/GaN MQWs (Sapphire)	$In_{0.2}Ga_{0.8}N$(2.5)/GaN(4.5) 3 periods (MOCVD)	50	2.235	Surficial GaN nanostructure	[103]
10	InGaN/GaN MQWs (Sapphire)	$In_{0.14}Ga_{0.86}N$(1.72)/GaN(4.14) 30 periods (MOCVD)	61	3.56	Improved MQW quality	[104]
11	Graded p-InGaN/InGaN/GaN MQWs/n-InGaN (Sapphire)	$In_{0.4}Ga_{0.6}N$(5)/GaN(10) 30 periods (MOCVD)	28	1.4	Graded p-InGaN&In-rich InGaN	[105]
12	InGaN/GaN MQWs (semi-polar GaN)	$In_{0.4}Ga_{0.56}N$(3)/GaN(9) 3 periods (MOCVD)	91.4	0.82	Semi-polar GaN substrate	[106]
13	p-AlGaN/InGaN/GaN MQWs (Sapphire)	$In_{0.25}Ga_{0.75}N$(2)/GaN(18) 10 periods (MOCVD)	5.8	0.259	Barrier thickness optimization	[107]
14	p-GaN/i-InGaN/n-GaN (Sapphire)	$In_{0.095}Ga_{0.905}N$(bulk 188) (MBE)	24.4	0.33	Bulk InGaN by MBE growth	[108]
15	InGaN/Al−N/GaN (Sapphire)	$In_{0.235}Ga_{0.765}N$(15)/Al−N(2 monolayers)/GaN(2.5) 6 periods (MBE)	N/A	1.75	Al−N passivation	[109]

GaN, with a wurtzite crystal structure, exhibit spontaneous polarization along the c-plane (0001) direction. Due to the lattice mismatch between InGaN and GaN, a strained InGaN layer grown on a GaN layer induces piezoelectric polarization. Both spontaneous and piezoelectric polarization contribute to the charge accumulation at the InGaN/GaN interfaces and the polarization-induced electric field, which affects the band structure and carrier collection of solar cells. The orientation of the spontaneous polarization points from nitrogen atoms to metal atoms along the c-axis [125]. Therefore, the orientation of the electric field induced by spontaneous polarization depends on the polarity of the grown layer (Ga-face or N-face). For the compressively strained InGaN layer grown on GaN, the orientation of the piezoelectric polarization is opposite to that of the spontaneous polarization. The collection of carriers is influenced by the built-in electric field and the polarization electric field. Considering both polarity and heterojunction structures, there are four types of solar cells (i.e., p-i-n with Ga-polar, p-i-n with N-polar, n-i-p with Ga-polar, and n-i-p with N-polar), as shown in Fig. 6(a) [126]. For the p-i-n with Ga-polar and the n-i-p with N-polar solar cells, the orientation of the built-in electric field and the polarization electric field is opposite. In this case, the polarization electric field raises the valence band offset and induces a high energy barrier height for holes, which prevents the collection of holes and reduces the current. On the contrary, in the p-i-n with N-polar and the n-i-p with Ga polar solar cells, the orientation of the two electric fields is the same, which facilitates carrier collection. In the conventional p-i-n with Ga-polar InGaN-based solar cells, the performance of solar cells is severely hindered by the polarization effect. To mitigate this influence, several structures can be adopted, including p-i-n with N-polar and n-i-p with Ga-polar solar cells [57,127,128], InGaN homojunction solar cells [129,130], and InGaN-based solar cells grown on nonpolar or semi-polar GaN substrates [29–31].

Li et al. [57] analyzed the effects of polarization on the PV performance of GaN/InGaN p-i-n solar cells using the APSYS software package. The J_{sc}, V_{oc}, and J–V curve of solar cells with different polarization charges were carefully studied. It was found that when interface charges were increased, J_{sc} decreased and V_{oc} increased slightly as shown in Fig. 6(b). They determined that the electric field created by the polarization charges was in the opposite direction of the built-in field, which hinders the drift and collection of holes and electrons and leads to a decrease of photocurrent and drop of the J-V curve. Meanwhile, with the increase of the interface charges, a drop formed in the hole Fermi level at the interface, which resulted in the increase of V_{oc}. Furthermore, they proposed that the PV properties of N-polar devices will not be affected by polarization due to the reversed direction of the polarization-induced field.

In addition to the design and study of the MQW absorbing layers, Huang et al. [29] have proposed a practical strategy to engineer the energy band structures of InGaN-based solar cells. They first adopted nonpolar m-plane and semipolar $(20\bar{2}1)$ plane bulk GaN substrates to demonstrate nonpolar and semipolar InGaN/GaN MQW solar cells. They reached the conclusion that the nonpolar and semipolar GaN crystal orientations could improve the PV performance of InGaN-based solar cells by systematically comparing the optical and electrical properties of the nonpolar, semipolar, and conventional polar devices. As shown in Fig. 6(c and d), nonpolar and semipolar devices have lower barrier heights than polar devices, which increases the tunneling rate of carriers and leads to better EQE. Therefore, the improvement in PV performance can be attributed to better carrier transport and collection in nonpolar m-plane devices, which reduced polarization effects. Compared with other methods such as increasing doping concentration, using nonpolar substrates is more practical, which paves a way for the broad application of III-nitride solar cells.

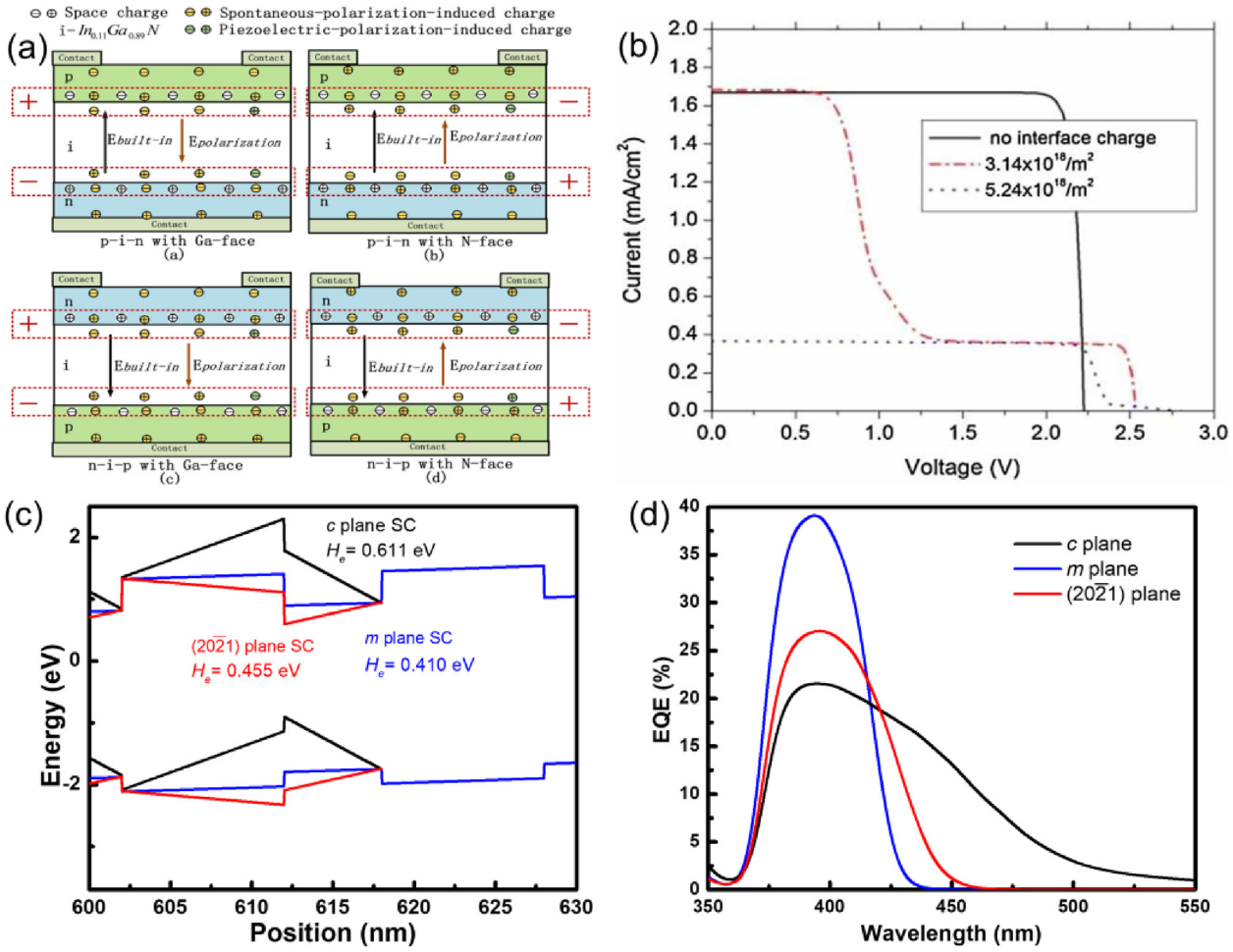

Fig. 6. The influence of polarization effect on InGaN-based solar cells. (a) Schematics showing polarization effects in four different InGaN/GaN structures. Reprint from Ref. [126] with permission. Copyright 2018, the Optical Society. (b) I–V curves for InGaN-based solar cells with different polarization charges. Reprint from Ref. [57] with permission. Copyright 2010, John Wiley and Sons. (c) Band diagrams and (d) EQE spectra for m-plane, (20$\bar{2}$1) plane, c-plane InGaN MQW solar cells. Reprint from Ref. [29] with permission. Copyright 2017, AIP Publishing.

4.2. Energy band engineering

The carrier transport mechanisms of MQW solar cells are affected by their energy band profile. Sayed et al. [84] have recently summarized the progress on quantum solar cells and reviewed the influence of energy levels on carrier transport. There are two main carrier transport approaches: thermionic emission and tunneling. Thin well thickness and low barrier heights are required to achieve thermionic emission, and a high possibility of tunneling can be obtained by using thin barrier thickness and low barrier heights. By tuning the composition of MQW, barrier and well thicknesses, and barrier heights, the transport approaches in MQW solar cells can be switched between thermionic emission and tunneling. As for InGaN-based solar cells, Lang et al. [131] reported that temperature-independent tunneling is dominant for thin barriers and temperature-dependent thermionic emission becomes prominent for thick barriers. These studies suggest that when analyzing the carrier dynamics of these devices, the structure and energy band profiles of the devices should be carefully considered.

In 2018 Huang et al. [54] devised a universal strategy for energy band engineering of InGaN MQW solar cells. As shown in Fig. 7, AlGaN electron and hole-blocking layers were incorporated into the device structure during MOCVD growth. The insertion of these blocking layers changed the band offset, which blocked the flow of carriers to the incorrect sides and facilitated the extraction of carriers. Time-resolved photoluminescence (TRPL) results suggest that the carrier lifetime on the solar cells with AlGaN layers increased by more than 40% compared to the reference sample, indicating greatly improved carrier collections. The J_{sc} of the solar cells also benefited from such design and increased by at least 46%. Furthermore, at high temperatures, solar cells with AlGaN layers also delivered superior PV performance to the reference devices. These results indicate band engineering with AlGaN layers in the InGaN MQW solar cell structures can effectively enhance the carrier collection process and is a promising design for InGaN-based solar cells with high PCE for both room temperature and high temperature PV applications.

4.3. Optical design

Optical design also plays a critical role in the PV performance of InGaN-based solar cells. Several groups have studied anti-reflection coating (ARC) designs that aim to improve the absorption of InGaN devices [132,133].

Lee et al. [132] compared the properties of InGaN-based solar cells with no ARC, a single-layer ARC, and a multiple-layer ARC. The ARC could improve transmittance and minimize reflectance in a broad range. Also, the multiple-layer ARC could serve as a

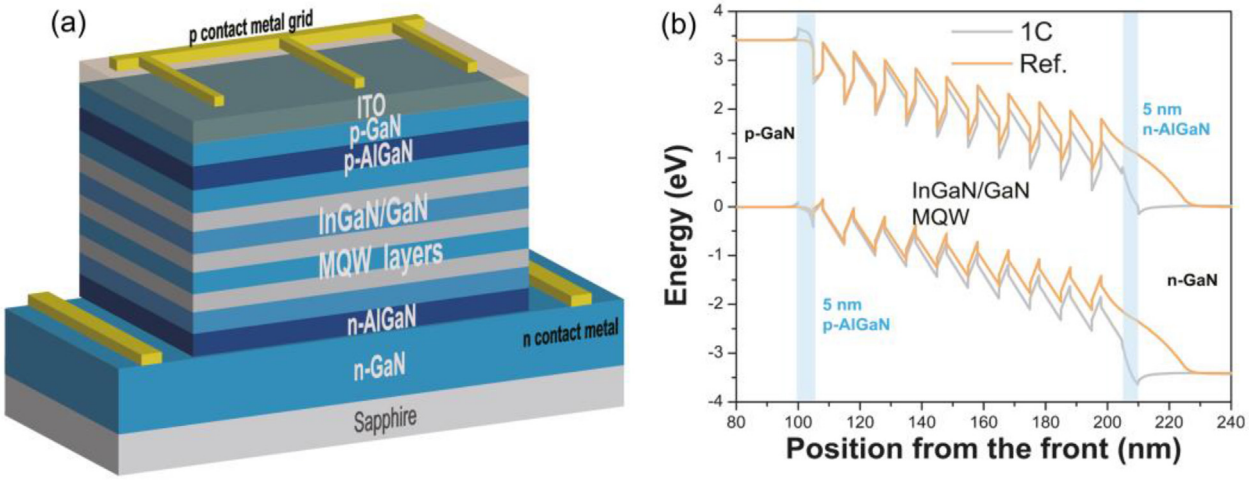

Fig. 7. Blocking layer design to improve the carrier collection. (a) The schematic device structure of the solar cells with electron- and hole-blocking layers and (b) the comparison between reference device and the device with blocking layers. Reprinted from Ref. [54] with permission. Copyright 2018, AIP Publishing.

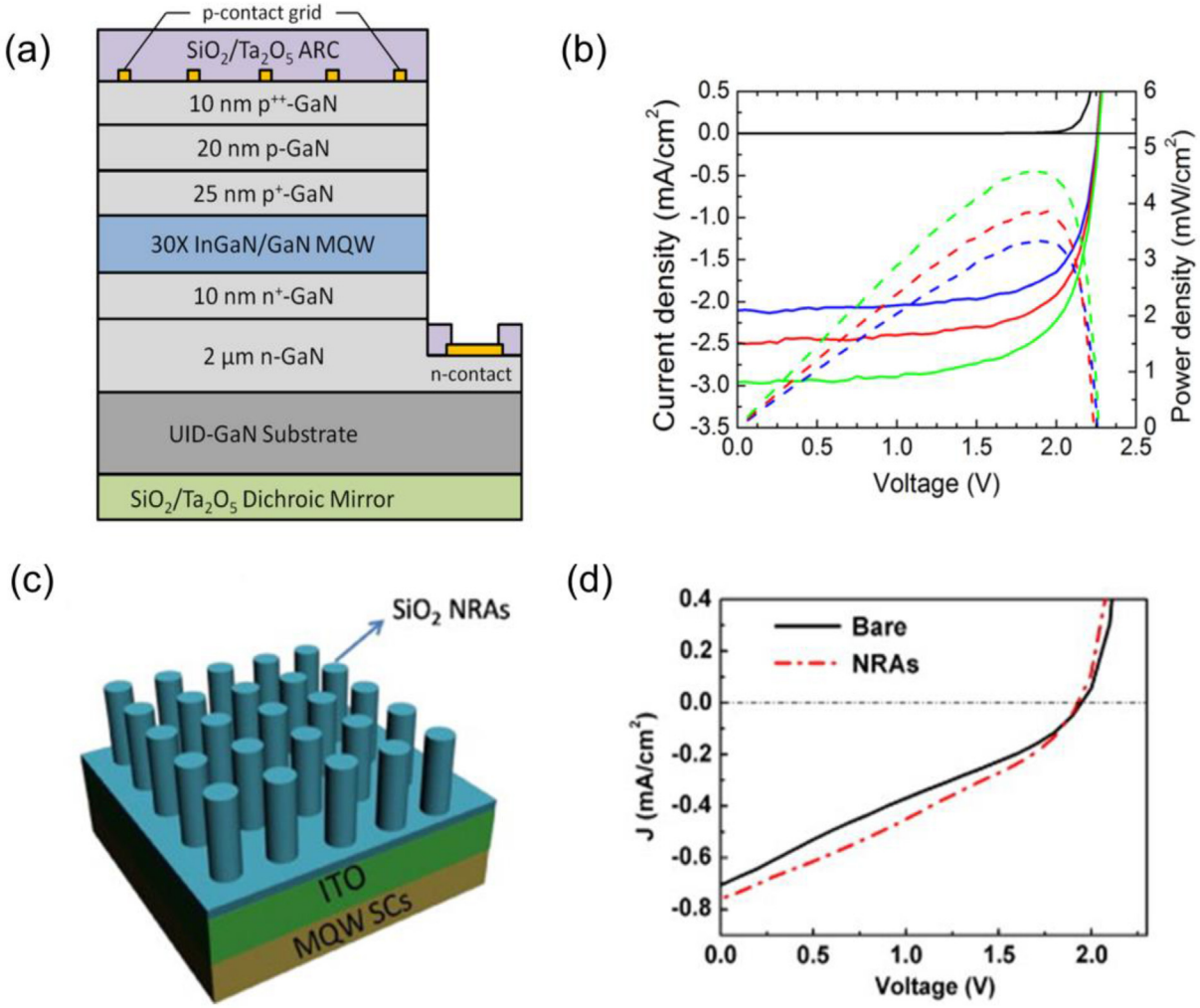

Fig. 8. Different optical design to enhance the light absorption (a) Schematic of the InGaN-based solar cells with contacts and optical coatings (b) EQE spectra, current density and power density as a function of voltage. Reprinted from Ref. [133] with permission. Copyright 2014, AIP Publishing. (c) Schematic of the InGaN-based solar cells with antireflective nanorod arrays (NRAs). (d) *J*–*V* characteristics of InGaN-based solar cells with NRAs. Reprinted from Ref. [38] with permission. Copyright 2012, Elsevier.

passivation layer to reduce the surface and edge recombination, which led to the suppression of current leakage and the increase in V_{oc}. Young et al. [133] investigated the use of optical coatings to improve the performance of multijunction solar cells, as shown in Fig. 8(a and b). The key was to maximize the light coupling for photons absorbed by the InGaN/GaN subcell while increasing the transmission of unabsorbed photons with lower energies. Thus, in addition to the application of an ARC on the top of the solar cell, a broadband dichroic mirror (DM) was coated on the backside to reflect the photons with low energies. The solar cells with both ARC and DM had higher EQE, J_{sc}, and PCE compared with solar cells without any coating or with only the ARC.

Others have employed nano-structured transparent conductive oxides to achieve a similar result [38,134–137]. For example, Ho et al. [38] grew antireflective SiO_2 nanorod arrays (NRAs) to reduce surface reflection, as shown in Fig. 8(c and d). Since the NRAs were much smaller than the incident light and the reflex index of SiO_2 (~1.56 at 400 nm), the NRAs could work as an effective medium since their effective reflex index of 1.36 is between air (~1) and ITO (~2.3). Furthermore, the space between NRAs had the potential to create a light trapping effect. The incident light that was diffracted by the surface of the NRAs, then propagated between NRAs before entering the MQW structure at a high angle enhanced light absorption with the increase in light propagation distance. As a result, the EQE and PCE of the solar cells were boosted due to the NRAs. Nevertheless, such optical designs on the nanoscale can also potentially deteriorate the electronic and optoelectronic properties if not done carefully since they require delicate and complicated device processing compared to conventional planar devices.

5. High-temperature performance

InGaN-based solar cells have demonstrated superior PV performance under both high irradiance [16,34,138–140] and high temperatures [13,30,33–35,141]. These reports have characterized and revealed the positive temperature coefficients of J_{sc}, FF, and PCE in certain ranges of temperatures and irradiances. In other words, the PCE of InGaN-based solar cells can increase with temperature under several hundred suns. In addition, they have also demonstrated superior thermal robustness after both thermal and irradiance cycling [35,142]. These unique features enable InGaN-based solar cells to be considered for high-temperature applications such as hybrid solar thermal-PV power plants and near-Sun space missions.

5.1. Positive temperature coefficient

High-temperature photovoltaics for terrestrial and extraterrestrial applications have presented challenges for current solar cell materials such as Si, III-V GaAs, and II-VI. Wide-bandgap III-nitride materials, in contrast, offer several intrinsic advantages that make them extremely appealing for high-temperature applications. Moses et al. [143] presented the change of properties of InGaN/GaN MQW solar cells under high irradiance and temperature. While V_{oc} increased with light intensity and dropped with temperature, J_{sc} increased with light intensity and temperature due to the narrowing of the bandgap under high temperature. Thus, the increase in J_{sc} could compensate for the decrease in V_{oc}, which resulted in greater PCE with increasing temperature under high irradiance of a few hundred suns, as shown in Fig. 9(a and b). The temperature

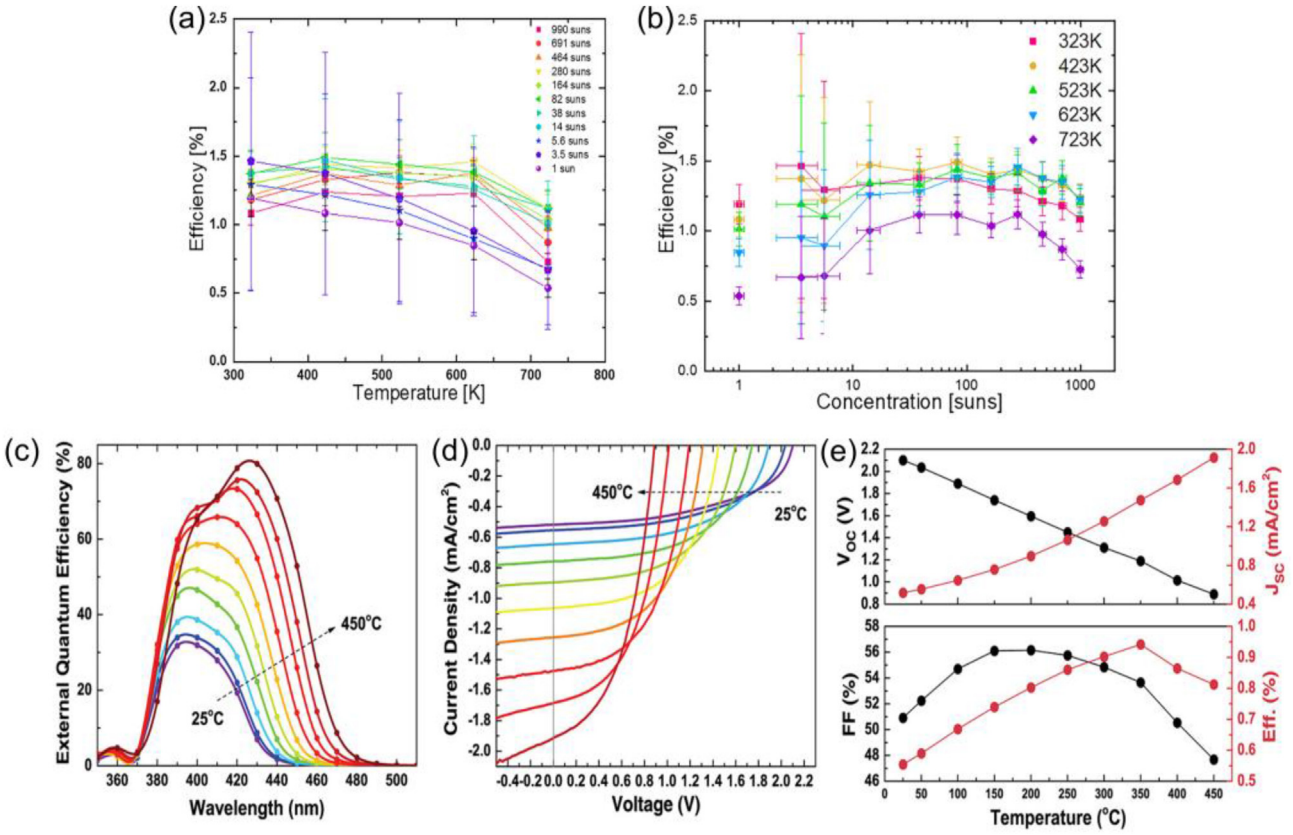

Fig. 9. The high temperature and high irradiance performance of InGaN-based solar cells. PCE of InGaN-based MQW solar cells as a function of (a) temperature and (b) irradiance concentration. Reprinted from Ref. [143] with permission. Copyright 2020, John Wiley and Sons. (c) EQE spectra. (d) *J–V* characteristics and (e) V_{oc}, J_{sc}, FF, and PCE values with different temperatures. Reprinted from Ref. [30] with permission. Copyright 2019, American Chemical Society.

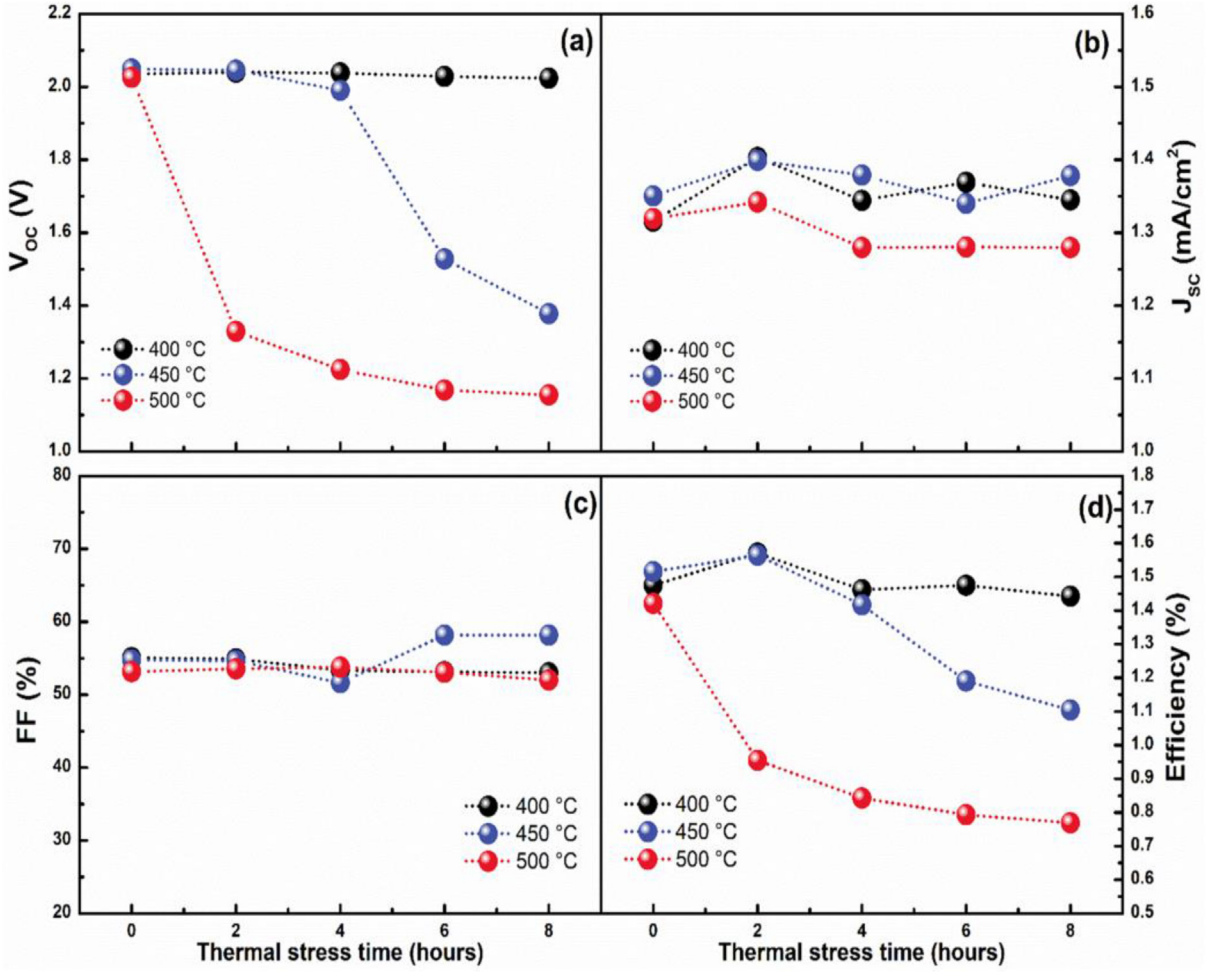

Fig. 10. The values of (a) V_{oc}, (b) J_{sc}, (c) FF, and (d) PCE of the InGaN-based solar cells under thermal stress. Reprinted from Ref. [35] with permission. Copy 2017, AIP Publishing.

coefficient, on the other hand, also depends on the quality of materials. Chen et al. [13] revealed that InGaN MQW solar cells on PSS had a positive temperature coefficient, although the solar cells on normal sapphire substrates exhibited a negative temperature coefficient. With the use of PSS, the edge dislocation densities were suppressed, which led to a decrease in non-radiative recombination centers and current leakage. The higher quality of MQW layers resulted in an increase in PCE with temperature.

Later, Huang et al. [30] fabricated nonpolar InGaN/GaN MQW solar cells with a positive temperature coefficient up to 350 °C. As demonstrated in Fig. 9(c–e), the peak EQE, J_{sc}, and PCE of the nonpolar devices showed a large enhancement from room temperature to 350 °C. The narrowed bandgap energy, broad absorption spectrum, improved MQW quality, and increased carrier lifetime and diffusion length contributed to this excellent performance at high temperatures. Moreover, III-nitride materials possessed a special self-cooling effect which was discovered using thermal radiation heat dissipation analysis. The superior thermal radiation ability of GaN led to increased heat dissipation, which reduced device temperatures. The self-cooling III-nitride solar cells can potentially be utilized in tandem cells as top cells to reduce the working temperature of the devices at high temperatures. These unique properties of III-nitrides make them good candidates for PV devices that need to function at elevated temperatures, such as in space missions and concentrating solar systems.

5.2. Thermal and optical stress measurement

In addition to *in-situ* measurements, Huang et al. [35] have also performed *ex-situ* thermal stress experiments to evaluate the thermal reliability and stability of InGaN MQW devices. They measured the thermal robustness of InGaN-based solar cells by applying thermal stress at different temperatures: 400 °C, 450 °C, and 500 °C. Fig. 10 presents the important features of the devices. J_{sc} and EQE show no degradation after thermal stress. Therefore, the severe decline in V_{oc} should be the main reason for the drop in PCE. The bad metal contacts are likely responsible for the PCE degradation because they change from Ohmic contacts to Schottky contacts after the thermal test, generating a large number of defects. In addition, the failure lifetime of solar cells under 300 °C is much longer than the lifetime under 325 °C or 350 °C. Therefore, metal contacts should be carefully treated and protected when designing and fabricating solar cells for high temperature applications.

Caria et al. [142] have carried out optical and thermal stress testing on InGaN/GaN MQW solar cells. Under increasing optical stress power, the device shows a low degradation with an increase in current density, and a slight reduction in V_{oc}. With an increasing temperature up to 175 °C, a decrease in V_{oc} and an increase in current density were witnessed. The degradation under constant long-term stress is partially recovered after storage, with a slight decrease in the voltage compared to the unstressed device. The

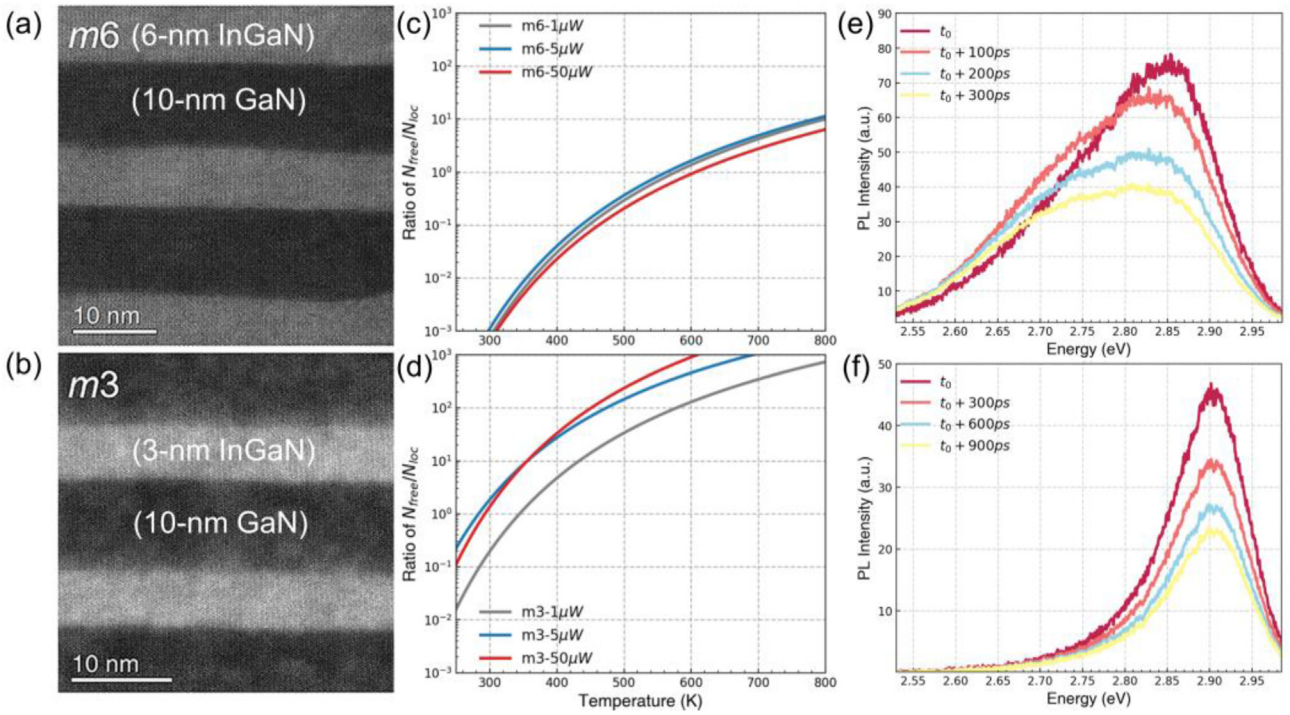

Fig. 11. Different carrier dynamics of m6 and m3 InGaN-based solar cells. (a) and (b) the STEM-HAADF images for m6 QW and barrier and m3 QW and barrier, respectively. (c) and (d) the ratio of density of free exciton and localized exciton for m6 and m3 solar cells, respectively (e) and (f) transient PL spectra for m6 and m3 solar cells, respectively. Reprinted from Ref. [31] with permission. Copyright 2020, Elsevier.

lowering in the voltage is possibly related to the increasing shunt resistance, while the increase in current density can be explained by the enhanced carrier generation and collection under optical and thermal stress.

5.3. Carrier dynamics under high temperature

While tremendous efforts have been put into the study of carrier dynamics of InGaN devices at relatively low temperatures [144–150], there are few reports analyzing the carrier dynamics at high temperatures. In order to better understand the distinctive and superior high-temperature performance of InGaN devices, Huang et al. [31] observed and explored anomalous carrier dynamics of two nonpolar *m*-plane InGaN/GaN QWs, one with a 6-nm InGaN/10-nm GaN QW (denoted as m6), and one with a 3-nm InGaN/10-nm GaN QW (denoted as m3). They used high-resolution scanning transmission electron microscopy (STEM)-cross-sectional high-angle annular dark-field (HAADF) to analyze the structures of two devices, as shown in Fig. 11(a and b). PL spectra revealed the behaviors of two different MQW solar cells at high temperatures, as shown in Fig. 11(c–f). For the m3 device, the fluctuation in Indium induced an interface between QWs and barriers, which reduced carrier localization and made carriers more vulnerable to the SRH recombination. The m6 device possessed a more uniform interface, and therefore better carrier confinement. This allowed for better radiative ability at high temperatures. Consequently, it is essential to improve the integrity and uniformity of QWs when fabricating the InGaN-based solar cells. These results provide insights into carrier dynamics at high temperatures, and will help to further increase the PCE of PV devices toward their theoretical limits.

6. Summary and future work

In summary, significant progress has been made both on fundamental understandings and engineering methods for InGaN-based solar cells. On the fundamental level, basic knowledge on the topics of loss mechanisms, carrier transports, polarization effects, and carrier dynamics at high temperatures have increased. On the device level, strategies for materials epitaxy and device fabrication were leveraged from the mature InGaN LED technologies. These efforts have led to the demonstration of nonpolar *m*-plane InGaN-based solar cells with quantum efficiency over 80% at 450 °C, a performance never-before seen on other solar cell material platforms. Despite this encouraging progress, more innovations in materials, devices, and integration schemes are still required to break through the PCE limit of current InGaN-based solar cells and expand their applications to more realistic settings.

On the materials level, one fundamental barrier to the performance of InGaN-based solar cells is the low indium composition (i.e., typically <20%) used in current devices. Due to the large lattice mismatch between InN and GaN (about 10% along *a*-direction and 9% along the *c*-direction) [148], it is very challenging to achieve InGaN layers with high indium compositions on GaN bulk templates. Furthermore, due to the constraints from material strain, very thin InGaN layers have been used in previous solar cell devices, which are detrimental to the photon absorption process. As a result, the current effective absorption spectra for InGaN-based solar cells are typically below 500 nm, limiting the photon energies that can be absorbed. It is therefore highly desirable to have thicker InGaN layers (e.g., >100 nm) with high indium compositions (e.g., >50%) to provide a better spectrum match and break the PCE limit of InGaN-based solar cells. Recent developments in InN epitaxy and InGaN bulk substrates are promising to address these challenges [69,71,108,149,150]. Moreover, recent progress made in MOCVD growth for producing InGaN LED wafers exhibiting amber and red emission colors can also be adopted for InGaN-based solar cell synthesis to further improve the spectrum match [151,152].

On the device level, it is critical to study the long-term reliability and high-temperature stability of InGaN-based solar cells, which are not well-understood. In previous studies, the carrier recombination of InGaN materials were only investigated at room

temperature or low-temperature conditions. Very recently, Huang et al. [31] investigated anomalous carrier dynamics of nonpolar *m*-plane InGaN/GaN QWs under high temperatures, which showed the carrier delocalization and phonon scattering mechanisms. Furthermore, another important topic of invitation is the degradation of metal contacts of InGaN-based solar cells under high temperature, which is a barrier for the reliability of InGaN-based solar cells. Although InGaN materials have shown good performance and high thermal stability, the metal contacts of InGaN-based solar cells degrade dramatically at high temperatures. Since InGaN-based solar cells will be widely used in extreme conditions, it is vital to understand the behavior of metal contacts at high temperatures. Huang et al. [35] analyzed the thermal stability of InGaN-based solar cells by applying thermal stress, which suggested that the deteriorated metal contacts are responsible for the degradation of the PCE of solar cells. However, more comprehensive investigations are required in order to design and fabricate high performance metal contacts for high-temperature InGaN-based solar cells.

On the integration and system level, it is desirable to integrate InGaN-based solar cells with existing multijunction solar cells such as GaAs-based III-V or Si solar cells to achieve over 50% efficiencies. However, InGaN materials are not compatible with GaAs materials in epitaxial growth. Currently, studies of InGaN tandem solar cells are mainly conducted through theoretical simulation or optically linked measurements. Novel methods in wafer bonding and solar cell integration should be explored to achieve electrically linked InGaN/III-V/Si multijunction solar cells. These innovations will help accelerate the applications of InGaN-based solar cells into more realistic conditions.

Credit author statement

Yuji Zhao: Supervision, Funding acquisition, Conceptualization, Writing-Original Draft, Writing-Reviewing and Editing.
Mingfei Xu: Conceptualization, Writing-Original Draft, Writing-Reviewing and Editing.
Xuanqi Huang: Conceptualization, Writing-Original Draft.
Justin Lebeau: Writing-Reviewing and Editing.
Tao Li: Writing-Reviewing and Editing.
Dawei Wang: Writing-Reviewing and Editing.
Houqiang Fu: Writing-Reviewing and Editing.
Kai Fu: Writing-Reviewing and Editing.
Xinqiang Wang: Writing-Reviewing and Editing.
Jingyu Lin: Writing-Reviewing and Editing.
Hongxing Jiang: Writing-Reviewing and Editing.

Declaration of competing interest

The authors declare that they have no known competing financial interests or personal relationships that could have appeared to influence the work reported in this paper.

Data availability

Data will be made available on request.

Acknowledgement

This research is supported as part of ULTRA, an Energy Frontier Research Center funded by the U.S. Department of Energy (DOE), Office of Science, Basic Energy Sciences (BES), under Award No. DE-SC0021230. The Mars surface and the satellite images in the graphical abstract are from NASA image and video library.

References

[1] S. Nakamura, T. Mukai, M. Senoh, Candela-class high-brightness InGaN/AlGaN double-heterostructure blue-light-emitting diodes, Appl. Phys. Lett. 64 (1994) 1687–1689, https://doi.org/10.1063/1.111832.
[2] Y. Zhao, H. Fu, G.T. Wang, S. Nakamura, Toward ultimate efficiency: progress and prospects on planar and 3D nanostructured nonpolar and semipolar InGaN light-emitting diodes, Adv. Opt. Photon 10 (2018) 246–308, https://doi.org/10.1364/AOP.10.000246.
[3] S. Nakamura, S. Pearton, G. Fasol, The Blue Laser Diode: the Complete Story, second ed., Springer, Berlin, Heidelberg, 2000.
[4] Y. Enya, et al., 531 nm Green lasing of ingan based laser diodes on semi-polar {2021} free-standing GaN substrates, Appl. Phys. Exp. 2 (2009), 082101, https://doi.org/10.1143/APEX.2.082101.
[5] U.K. Mishra, P. Parikh, Y.F. Wu, AlGaN/GaN HEMTs - an overview of device operation and applications, Proc. IEEE 90 (2022) 1022–1031, https://doi.org/10.1109/JPROC.2002.1021567.
[6] U.K. Mishra, L. Shen, T.E. Kazior, Y.F. Wu, GaN-based RF power devices and amplifiers, Proc. IEEE 96 (2008) 287–305, https://doi.org/10.1109/JPROC.2007.911060.
[7] B.J. Baliga, Gallium nitride devices for power electronic applications, Semicond. Sci. Technol. 28 (2013), 074011, https://doi.org/10.1088/0268-1242/28/7/074011.
[8] K. Fu, H. Fu, X. Huang, H. Chen, T.-H. Yang, J. Montes, C. Yang, J. Zhou, Y. Zhao, Demonstration of 1.27 kV etch-then-regrow GaN p-n junctions with low leakage for GaN power electronics, IEEE Electron. Device Lett. 40 (2019) 1728–1731, https://doi.org/10.1109/LED.2019.2941830.
[9] J. Wu, Unusual properties of the fundamental band gap of InN, Appl. Phys. Lett. 80 (2002) 3967–3969, https://doi.org/10.1063/1.1482786.
[10] J. Wu, When group-III nitrides go infrared: new properties and perspectives, J. Appl. Phys. 106 (2009), 011101, https://doi.org/10.1063/1.3155798.
[11] C.J. Neufeld, C.C. Samantha, R.M. Farrell, M. Iza, S. Keller, S. Nakamura, S.P. DenBaars, J.S. Speck, U.K. Mishra, Observation of positive thermal power coefficient in InGaN/GaN quantum well solar cells, Appl. Phys. Lett. 99 (2011), 071104, https://doi.org/10.1063/1.3624850.
[12] L. Zhao, T. Detchprohm, C. Wetzel, High 400°C operation temperature blue spectrum concentration solar junction in GaInN/GaN, Appl. Phys. Lett. 105 (2014), 243903, https://doi.org/10.1063/1.4904717.
[13] Z. Chen, et al., Positive temperature coefficient of photovoltaic efficiency in solar cells based on InGaN/GaN MQWs, Appl. Phys. Lett. 109 (2016), 062104, https://doi.org/10.1063/1.4960765.
[14] J. Wu, W. Walukiewicz, K.M. Yu, W. Shan, J.W. Ager III, Superior radiation resistance of $In_{1-x}Ga_xN$ alloys: full-solar-spectrum photovoltaic material system, J. Appl. Phys. 94 (2003) 6477–6482, https://doi.org/10.1063/1.1618353.
[15] H.M. Branz, W. Regan, K.J. Gerst, J.B. Borak, E.A. Santori, Hybrid solar converters for maximum exergy and inexpensive dispatchable electricity, Energy Environ. Sci. 8 (2015) 3083–3091, https://doi.org/10.1039/C5EE01998B.
[16] R. Dahal, J. Li, K. Aryal, J.Y. Lin, H.X. Jiang, InGaN/GaN multiple quantum well concentrator solar cells, Appl. Phys. Lett. 97 (2010), 073115, https://doi.org/10.1063/1.3481424.
[17] Y. Zhao, X. Huang, H. Fu, H. Chen, Z. Liu, J. Montes, I. Baranowski, InGaN-Based Solar Cells for Space Applications, in: 2017 IEEE 60th International Midwest Symposium on Circuits and Systems (MWSCAS), Medford, United States, 2017, pp. 954–957, https://doi.org/10.1109/MWSCAS.2017.8053083.
[18] O. Jani, I. Ferguson, C. Honsberg, S. Kurtz, Design and characterization of GaN/InGaN solar cells, Appl. Phys. Lett. 91 (2007), 132117, https://doi.org/10.1063/1.2793180.
[19] C.J. Neufeld, N.G. Toledo, S.C. Cruz, M. Iza, S.P. DenBaars, U.K. Mishra, High quantum efficiency InGaN/GaN solar cells with 2.95 eV band gap, Appl. Phys. Lett. 93 (2008), 143502, https://doi.org/10.1063/1.2988894.
[20] R.-H. Horng, S.-T. Lin, Y.-L. Tsai, M.-T. Chu, W.-Y. Liao, M.-H. Wu, R.-M. Lin, Y.-C. Lu, Improved conversion efficiency of GaN/InGaN thin-film solar cells, IEEE Electron. Device Lett. 30 (2009) 724–726, https://doi.org/10.1109/LED.2009.2021414.
[21] R. Dahal, B. Pantha, J. Li, J.Y. Lin, H.X. Jiang, InGaN/GaN multiple quantum well solar cells with long operating wavelengths, Appl. Phys. Lett. 94 (2009), 063505, https://doi.org/10.1063/1.3081123.
[22] R.M. Farrell, et al., High quantum efficiency InGaN/GaN multiple quantum well solar cells with spectral response extending out to 520 nm, Appl. Phys. Lett. 98 (2011), 201107, https://doi.org/10.1063/1.3591976.
[23] Y. Kuwahara, et al., GaInN-based solar cells using strained-layer GaInN/GaInN superlattice active layer on a freestanding GaN substrate, Appl. Phys. Express 4 (2011), 021001, https://doi.org/10.1143/APEX.4.021001.
[24] S. Liu, Q. Wang, H. Xiao, K. Wang, C. Wang, X. Wang, W. Ge, Z. Wang, Optimization of growth and fabrication techniques to enhance the InGaN/GaN multiple quantum well solar cells performance, Superlattices Microstruct. 109 (2017) 194–200, https://doi.org/10.1016/j.spmi.2017.05.014.
[25] V. Fiorentini, F. Bernardini, F.D. Sala, A.D. Carlo, P. Lugli, Effects of macroscopic polarization in III-V nitride multiple quantum wells, Phys. Rev. B 60 (1999) 8849, https://doi.org/10.1103/PhysRevB.60.8849.
[26] P. Walterweit, O. Brandt, A. Trampert, H.T. Grahn, J. Menniger, M. Ramsteiner, M. Reiche, K.H. Ploog, Nitride semiconductors free of electrostatic fields for efficient white light-emitting diodes, Nature 406 (2000) 865–868, https://doi.org/10.1038/35022529.

[27] C.A.M. Fabien, M. Moseley, B. Gunning, W.A. Doolittle, A.M. Fischer, Y.O. Wei, F.A. Ponce, Simulations, Practical limitations, and novel growth technology for InGaN-based solar cells, IEEE J. Photovoltaics 4 (2016) 601–606, https://doi.org/10.1109/JPHOTOV.2013.2292748.

[28] C.A.M. Fabien, W.A. Doolittle, Guidelines and limitations for the design of high-efficiency InGaN single-junction solar cells, Sol. Energy Mater. Sol. Cells 130 (2014) 354–363, https://doi.org/10.1016/j.solmat.2014.07.018.

[29] X. Huang, et al., Nonpolar and semipolar InGaN/GaN multiple-quantum-well solar cells with improved carrier collection efficiency, Appl. Phys. Lett. 110 (2017), 161105, https://doi.org/10.1063/1.4980139.

[30] X. Huang, et al., High-temperature polarization-free III-nitride solar cells with self-cooling effects, ACS Photon. 6 (2019) 2096–2103, https://doi.org/10.1021/acsphotonics.9b00655.

[31] X. Huang, et al., Anomalous carrier dynamics and localization effects in nonpolar m-plane InGaN/GaN quantum wells at high temperatures, Nano Energy 76 (2020), 105013, https://doi.org/10.1016/j.nanoen.2020.105013.

[32] G.F. Brown, J.W. Ager, W. Walukiewicz, J. Wu, Finite element simulations of compositionally graded InGaN solar cells, Sol. Energy Mater. Sol. Cells 94 (2010) 478–483, https://doi.org/10.1016/j.solmat.2009.11.010.

[33] J.J. Williams, et al., Refractory $In_xGa_{1-x}N$ solar cells for high-temperature applications, IEEE J. Photovoltaics 7 (2017) 1646–1652, https://doi.org/10.1109/JPHOTOV.2017.2756057.

[34] D.-H. Lien, Y.-H. Hsiao, S.-G. Yang, M.-L. Tsai, T.-C. Wei, S.-C. Lee, J.-H. He, Harsh photovoltaics using InGaN/GaN multiple quantum well schemes, Nano Energy 11 (2015) 104–109, https://doi.org/10.1016/j.nanoen.2014.10.013.

[35] X. Huang, et al., Reliability analysis of InGaN/GaN multi-quantum-well solar cells under thermal stress, Appl. Phys. Lett. 111 (2017), 233511, https://doi.org/10.1063/1.5006650.

[36] S.A. Kazazis, E. Papadomanolaki, M. Androulidaki, M. Kayambaki, E. Iliopoulos, Optical properties of InGaN thin films in the entire composition range, J. Appl. Phys. 123 (2018), 125101, https://doi.org/10.1063/1.5020988.

[37] D.S. Arteev, A.V. Sakharov, E.E. Zavarin, W.V. Lundin, A.N. Smirnov, V.Y. Davydov, M.A. Yagovkina, S.O. Usov, A.F. Tsatsulnikov, Investigation of statistical broadening in InGaN alloys, J. Phys. Conf. Ser. 1135 (2018), 012050, https://doi.org/10.1088/1742-6596/1135/1/012050.

[38] C.H. Ho, G.J. Lin, P.H. Fu, C.A. Lin, P.C. Yang, I.-M. Chan, K.Y. Lai, J.H. He, An efficient light-harvesting scheme using SiO_2 nanorods for InGaN multiple quantum well solar cells, Sol. Energy Mater. Sol. Cells 103 (2012) 194–198, https://doi.org/10.1016/j.solmat.2012.04.007.

[39] L. Li, Y. Zhang, S. Xu, W. Bi, Z.-H. Zhang, H.-C. Kuo, On the hole injection for III-nitride based deep ultraviolet light-emitting diodes, Materials 10 (2017) 1221, https://doi.org/10.3390/ma10101221.

[40] L.J. Lin, Y.-P. Chiou, Optical design of GaN/$In_xGa_{1-x}N$/cSi tandem solar cells with triangular diffraction grating, Opt Express 23 (2015) A614–A624, https://doi.org/10.1364/OE.23.00A614.

[41] S. Lai, Q. Li, H. Long, L. Ying, Z. Zheng, B. Zhang, Theoretical study and optimization of the green InGaN/GaN multiple quantum wells with pre-layer, Superlattice. Microst. 155 (2021), 106906, https://doi.org/10.1016/j.spmi.2021.106906.

[42] H. Woo, Y. Jo, J. Kim, S. Cho, C.H. Roh, J.H. Lee, H. Kim, C.-K. Hahn, H. Im, Correlation between pit formation and phase separation in thick InGaN film on a Si substrate, Curr. Appl. Phys. 18 (2018) 1558–1563, https://doi.org/10.1016/j.cap.2018.10.002.

[43] N.G. Toledo, U.K. Mishra, InGaN solar cell requirements for high-efficiency integrated III-nitride/non-III-nitride tandem photovoltaic devices, J. Appl. Phys. 111 (2012), 114505, https://doi.org/10.1063/1.4723831.

[44] L. Hsu, W. Walukiewicz, Modeling of InGaN/Si tandem solar cells, J. Appl. Phys. 104 (2008), 024507, https://doi.org/10.1063/1.2952031.

[45] S.W. Feng, C.M. Lai, C.H. Chen, W.C. Sun, L.W. Tu, Theoretical simulations of the effects of the indium content, thickness, and defect density of the i-layer on the performance of p-i-n InGaN single homojunction solar cells, J. Appl. Phys. 108 (2010), 093118, https://doi.org/10.1063/1.3484040.

[46] A. Asgari, K. Khalili, Temperature dependence of InGaN/GaN multiple quantum well based high efficiency solar cell, Sol. Energy Mater. Sol. Cells 95 (2011) 3124–3129, https://doi.org/10.1016/j.solmat.2011.07.001.

[47] N. Cavassilas, F. Michelini, M. Bescond, Theoretical comparison of multiple quantum wells and thick-layer designs in InGaN/GaN solar cells, Appl. Phys. Lett. 105 (2014), 063903, https://doi.org/10.1063/1.4893024.

[48] R. Belghouthi, S. Taamalli, F. Echouchene, H. Mejri, H. Belmabrouk, Modeling of polarization charge in N-face InGaN/GaN MQW solar cells, Mater. Sci. Semicond. Process. 40 (2015) 424–428, https://doi.org/10.1016/j.mssp.2015.07.009.

[49] X. Huang, H. Fu, H. Chen, Z. Lu, D. Ding, Y. Zhao, Analysis of loss mechanisms in InGaN solar cells using a semi-analytical model, J. Appl. Phys. 119 (2016), 213101, https://doi.org/10.1063/1.4953006.

[50] K.F. Chen, C.L. Hung, Numerical study of InGaN tandem solar cells with intermediate bands, Phys. Status Solidi Rapid Res. Lett. 11 (2017), 1600429, https://doi.org/10.1002/pssr.201600429.

[51] A. Adaine, S.O.S. Hamady, N. Fressengeas, Effects of structural defects and polarization charges in InGaN-based double-junction solar cell, Superlattices Microstruct. 107 (2017) 267–277, https://doi.org/10.1016/j.spmi.2017.04.025.

[52] S. Wu, L. Cheng, Q. Wang, Effects of the unintentional background concentration, indium composition and defect density on the performance of InGaN p-i-n homojunction solar cells, Superlattices Microstruct. 119 (2018) 9–18, https://doi.org/10.1016/j.spmi.2018.04.033.

[53] G. Siddharth, V. Garg, B.S. Sengar, R. Bhardwaj, P. Kumar, S. Mukherjee, Analytical study of performance parameters of inGaN/GaN multiple quantum well solar cell, IEEE Trans. Electron. Dev. 66 (2019) 3399–3404, https://doi.org/10.1109/TED.2019.2920934.

[54] X. Huang, et al., Energy band engineering of InGaN/GaN multi-quantum-well solar cells via AlGaN electron- and hole-blocking layers, Appl. Phys. Lett. 113 (2018), 043501, https://doi.org/10.1063/1.5028530.

[55] J.-Y. Wang, F.-J. Tsai, J.-J. Huang, C.-Y. Chen, N. Li, Y.-W. Kiang, C.C. Yang, Enhancing InGaN-based solar cell efficiency through localized surface plasmon interaction by embedding Ag nanoparticles in the absorbing layer, Opt Express 18 (2010) 2682–2694, https://doi.org/10.1364/OE.18.002682.

[56] J.Y. Chang, Y.K. Kuo, Numerical study on the influence of piezoelectric polarization on the performance of p-on-n (0001)-face GaN/InGaN p-i-n solar cells, IEEE Electron. Device Lett. 32 (2011) 937–939, https://doi.org/10.1109/LED.2011.2150195.

[57] Z.Q. Li, M. Lestradet, Y.G. Xiao, S. Li, Effects of polarization charge on the photovoltaic properties of InGaN solar cells, Phys. Status Solidi A 208 (2011) 928–931, https://doi.org/10.1002/pssa.201026489.

[58] A.T.M. Golam Sarwar, R.C. Myers, Exploiting piezoelectric charge for high performance graded InGaN nanowire solar cells, Appl. Phys. Lett. 101 (102) (2012), 143905, https://doi.org/10.1063/1.4757990.

[59] Y.-C. Yao, M.-T. Tsai, C.-Y. Huang, T.-Y. Lin, J.-K. Sheu, Y.-J. Lee, Efficient collection of photogenerated carriers by inserting double tunnel junctions in III-nitride p-i-n solar cells, Appl. Phys. Lett. 103 (2013), 193503, https://doi.org/10.1063/1.4829443.

[60] J.Y. Chang, S.H. Yen, Y.A. Chang, Y.K. Kuo, Simulation of high-efficiency GaN/InGaN p-i-n solar cell with suppressed polarization and barrier effects, IEEE J. Quant. Electron. 49 (2013) 17–23, https://doi.org/10.1109/JQE.2012.2225601.

[61] S. Lee, Y. Honda, H. Amano, Effect of piezoelectric field on carrier dynamics in InGaN-based solar cells, J. Phys. D Appl. Phys. 49 (2015), 025103, https://doi.org/10.1088/0022-3727/49/2/025103.

[62] Y. Fang, H. McFavilen, D. Ding, D. Vasileska, S.M. Goodnick, Simulation of the High Temperature Performance of InGaN Multiple Quantum Well Solar Cells, in: IEEE 43rd Photovoltaic Specialists Conference (PVSC), Portland, United States, 2016, pp. 1138–1141, https://doi.org/10.1109/PVSC.2016.7749792.

[63] W. El-Huni, A. Migan, D. Alamarguy, Z. Djebbour, Modeling of InGaN/Si tandem cells: comparison between 2-contacts/4-contacts, EPJ Photovoltaics 8 (2017), 85502, https://doi.org/10.1051/epjpv/2017003.

[64] M.J. Jeng, Y.L. Lee, L.B. Chang, Temperature dependences of $In_xGa_{1-x}N$ multiple quantum well solar cells, J. Phys. D Appl. Phys. 42 (2009), 105101, https://doi.org/10.1088/0022-3727/42/10/105101.

[65] G. Namkoong, P. Boland, S.-Y. Bae, J.-P. Shim, D.-S. Lee, S.-R. Jeon, K. Foe, K. Latimer, W.A. Doolittle, Effect of III-nitride polarization on V_{OC} in p-i-n and MQW solar cells, Phys. Status Solidi Rapid Res. Lett. 5 (2011) 86–88, https://doi.org/10.1002/pssr.201004512.

[66] E.A. Clinton, et al., A Review of the Synthesis of Reduced Defect Density InxGa1−xN for All Indium Compositions, Solid State Electron. 136 (2017) 3–11, https://doi.org/10.1016/j.sse.2017.06.020.

[67] A.K. Tan, N.A. Hamzah, M.A. Ahmad, S.S. Ng, Z. Hassan, Recent advances and challenges in the MOCVD growth of indium gallium nitride: a brief review, Mater. Sci. Semicond. Process. 143 (2022), 106545, https://doi.org/10.1016/j.mssp.2022.106545.

[68] M.R. Islam, M.R. Kaysir, M.J. Islam, A. Hashimoto, A. Yamamoto, MOVPE growth of $In_xGa_{1-x}N$ (x ~ 0.4) and fabrication of homo-junction solar cells, J. Mater. Sci. Technol. 29 (2013) 128–136, https://doi.org/10.1016/j.jmst.2012.12.005.

[69] A. Koukitu, H. Seki, Thermodynamic study on phase separation during MOVPE growth of $In_xGa_{1-x}N$, J. Cryst. Growth 189 (1998) 13–18, https://doi.org/10.1016/S0022-0248(98)00147-X.

[70] O. Jani, H. Yu, E. Trybus, B. Jampana, I. Ferguson, A. Doolittle, C. Honsberg, Effect of Phase Separation on Performance of III-V Nitride Solar Cells, in: Proceedings of the 22nd European Photovoltaic Solar Energy Conference, Milan, Italy, 2007, pp. 64–67.

[71] H. Komaki, R. Katayama, K. Onabe, M. Ozeki, T. Ikari, Nitrogen supply rate dependence of InGaN growth properties, by RF-MBE, J. Cryst. Growth 305 (2007) 12–18, https://doi.org/10.1016/j.jcrysgro.2007.01.044.

[72] R. Togashi, T. Kamoshita, Y. Nishizawa, H. Murakami, Y. Kumagai, A. Koukitu, Experimental and ab-initio studies of temperature dependent InN decomposition in various ambient, Phys. Status Solidi C 5 (2008) 1518–1521, https://doi.org/10.1002/pssc.200778434.

[73] A. Yamamoto, T.M. Hasan, K. Kodama, N. Shigekawa, M. Kuzuhara, Growth temperature dependent critical thickness for phase separation in thick (~1 μm) In_x $Ga_{1-x}N$ (x=0.2-0.4), J. Cryst. Growth 419 (2015) 64–68, https://doi.org/10.1016/j.jcrysgro.2015.02.100.

[74] S.Y. Karpov, Suppression of phase separation in InGaN due to elastic strain, MRS Internet J. Nitride Semicond. Res. 3 (1998) 16, https://doi.org/10.1557/S1092578300000880.

[75] R. Singh, D. Doppalapudi, T.D. Moustakas, L.T. Romano, Phase separation in InGaN thick films and formation of InGaN/GaN double heterostructures in

the entire alloy composition, Appl. Phys. Lett. 70 (1997) 1089–1091, https://doi.org/10.1063/1.118493.
[76] G. Namkoong, E. Trybus, K.K. Lee, M. Moseley, W.A. Doolittle, D.C. Look, Metal modulation epitaxy growth for extremely high hole concentrations above 10^{19} cm^{-3} in GaN, Appl. Phys. Lett. 93 (2008) 17–20, https://doi.org/10.1063/1.3005640.
[77] C.A.M. Fabien, B.P. Gunning, W.A. Doolittle, A.M. Fischer, Y.O. Wei, H. Xie, F.A. Ponce, Low-temperature growth of InGaN films over the entire composition range by MBE, J. Cryst. Growth 425 (2015) 115–118, https://doi.org/10.1016/j.jcrysgro.2015.02.014.
[78] C.F. Johnston, M.J. Kappers, C.J. Humphreys, Microstructural evolution of nonpolar (11-20) GaN grown on (1-102) sapphire using a 3D-2D method, J. Appl. Phys. 105 (2009), 073102, https://doi.org/10.1063/1.3103305.
[79] C. Yang, et al., Photovoltaic effects in InGaN structures with p-n junctions, Phys. Status Solidi A 204 (2007) 4288–4291, https://doi.org/10.1002/pssa.200723202.
[80] S.W. Zeng, B.P. Zhang, J.W. Sun, J.F. Cai, C. Chen, J.Z. Yu, Substantial photoresponse of InGaN p-i-n homojunction solar cells, Semicond. Sci. Technol. 24 (2009), 055009, https://doi.org/10.1088/0268-1242/24/5/055009.
[81] B.R. Jampana, A.G. Melton, M. Jamil, N.N. Faleev, R.L. Opila, I.T. Ferguson, C.B. Honsberg, Design and realization of wide-band-gap (~ 2.67 eV) InGaN p-n junction solar cell, IEEE Electron. Device Lett. 31 (2010) 32–34, https://doi.org/10.1109/LED.2009.2034280.
[82] J.P. Shim, S.R. Jeon, Y.K. Jeong, D.S. Lee, Improved efficiency by using transparent contact layers in InGaN-based p-i-n solar cells, IEEE Electron. Device Lett. 31 (2010) 1140–1142, https://doi.org/10.1109/LED.2010.2058087.
[83] P. Misra, C. Boney, N. Medelci, D. Starikov, A. Freundlich, A. Bensaoula, Fabrication and Characterization of 2.3eV InGaN Photovoltaic Devices, in: 33rd IEEE Photovoltaic Specialists Conference (PVSC), San Diego, United States, 2008, pp. 1–5, https://doi.org/10.1109/PVSC.2008.4922693.
[84] I. Sayed, S.M. Bedair, Quantum well solar cells: principles, recent progress, and potential, IEEE J. Photovoltaics 9 (2019) 402–423, https://doi.org/10.1109/JPHOTOV.2019.2892079.
[85] A. Mukhtarova, S. Valdueza-Felip, L. Redaelli, C. Durand, C. Bougerol, E. Monroy, J. Eymery, Dependence of the photovoltaic performance of pseudomorphic InGaN/GaN multiple-quantum-well solar cells on the active region thickness, Appl. Phys. Lett. 108 (2016), 161907, https://doi.org/10.1063/1.4947445.
[86] L. Redaelli, et al., Effect of the quantum well thickness on the performance of InGaN photovoltaic cells, Appl. Phys. Lett. 105 (2014), 131105, https://doi.org/10.1063/1.4896679.
[87] M. Miyoshi, T. Tsutsumi, T. Kabata, T. Mori, T. Egawa, Effect of well layer thickness on quantum and energy conversion efficiencies for InGaN/GaN multiple quantum well solar cells, Solid State Electron. 129 (2017) 29–34, https://doi.org/10.1016/j.sse.2016.12.009.
[88] L. Redaelli, A. Mukhtarova, A. Ajay, A. Núñez-Cascajero, S. Valdueza-Felip, J. Bleuse, C. Durand, J. Eymery, E. Monroy, Effect of the barrier thickness on the performance of multiple-quantum-well InGaN photovoltaic cells, Jpn. J. Appl. Phys. 54 (2015), 072302, https://doi.org/10.7567/JJAP.54.072302.
[89] J.J. Wierer, D.D. Koleske, S.R. Lee, Influence of barrier thickness on the performance of InGaN/GaN multiple quantum well solar cells, Appl. Phys. Lett. 100 (2012), 111119, https://doi.org/10.1063/1.3695170.
[90] N. Watanabe, H. Yokoyama, N. Shigekawa, K.I. Sugita, A. Yamamoto, Barrier thickness dependence of photovoltaic characteristics of InGaN/GaN multiple quantum well solar cells, Jpn. J. Appl. Phys. 51 (2012) 10ND10, https://doi.org/10.1143/JJAP.51.10ND10.
[91] J. Lin, Y. Yu, Z. Zhang, F. Gao, S. Liu, W. Wang, G. Li, A novel approach for achieving high-efficiency photoelectrochemical water oxidation in InGaN nanorods grown on Si system: MXene nanosheets as multifunctional interfacial modifier, Adv. Funct. Mater. 30 (2020), 1910479, https://doi.org/10.1002/adfm.201910479.
[92] J. Lin, W. Wang, G. Li, Modulating surface/interface structure of emerging InGaN nanowires for efficient photoelectrochemical water splitting, Adv. Funct. Mater. 30 (2020), 2005677, https://doi.org/10.1002/adfm.202005677.
[93] U. Chatterjee, J.-H. Park, D.-Y. Um, C.-R. Lee, III-nitride nanowires for solar light harvesting: a review, Renew. Sustain. Energy Rev. 79 (2017) 1002–1015, https://doi.org/10.1016/j.rser.2017.05.136.
[94] L. Hrachowina, Y. Chen, E. Barrigón, R. Wallenberg, M.T. Borgström, Realization of axially defined GaInP/InP/InAsP triple-junction photovoltaic nanowires for high-performance solar cells, Mater. Today Energy 27 (2022), 101050, https://doi.org/10.1016/j.mtener.2022.101050.
[95] H.P.T. Nguyen, S. Zhang, K. Cui, X. Han, S. Fathololoumi, M. Couillard, G.A. Botton, Z. Mi, P-type modulation doped InGaN/GaN dot-in-a-wire white-light-emitting diodes monolithically grown on Si(111), Nano Lett. 11 (2011) 1919–1924, https://doi.org/10.1021/nl104536x.
[96] S. Zhao, H.P.T. Nguyen, M.G. Kibria, Z. Mi, III-Nitride nanowire optoelectronics, Prog. Quant. Electron. 44 (2015) 14–68, https://doi.org/10.1016/j.pquantelec.2015.11.001.
[97] M. Miyoshi, M. Ohta, T. Mori, T. Egawa, A comparative study of InGaN/GaN multiple-quantum-well solar cells grown on sapphire and AlN template by metalorganic chemical vapor deposition, Phys. Status Solidi A 215 (2017), 1700323, https://doi.org/10.1002/pssa.201700323.
[98] H. Shan, B. Chen, X. Li, Z. Lin, S. Xu, Y. Hao, J. Zhang, The performance enhancement of an InGaN/GaN multiple-quantum-well solar cell by superlattice structure, Jpn. J. Appl. Phys. 56 (2017), 110305, https://doi.org/10.7567/JJAP.56.110305.
[99] C. Jiang, et al., Enhanced photocurrent in InGaN/GaN MQWs solar cells by coupling plasmonic with piezo-phototronic effect, Nano Energy 57 (2019) 300–306, https://doi.org/10.1016/j.nanoen.2018.12.036.
[100] C. Jiang, L. Jing, X. Huang, M. Liu, C. Du, T. Liu, X. Pu, W. Hu, Z.L. Wang, Enhanced solar cell conversion efficiency of InGaN/GaN multiple quantum wells by piezo-phototronic effect, ACS Nano 11 (2017) 9405–9412, https://doi.org/10.1021/acsnano.7b04935.
[101] E. Vadiee, et al., InGaN solar cells with regrown GaN homojunction tunnel contacts, Appl. Phys. Express 11 (2018), 082304, https://doi.org/10.7567/APEX.11.082304.
[102] M. Arif, et al., Improving InGaN heterojunction solar cells efficiency using a semibulk absorber, Sol. Energy Mater. Sol. Cells 159 (2017) 405–411, https://doi.org/10.1016/j.solmat.2016.09.030.
[103] Z. Bi, D. Bacon-Brown, F. Du, J. Zhang, S. Xu, P. Li, J. Zhang, Y. Zhan, Y. Hao, An InGaN/GaN MQWs solar cell improved by a surficial GaN nanostructure as light traps, IEEE Photon. Technol. Lett. 30 (2018) 83–86, https://doi.org/10.1109/LPT.2017.2775706.
[104] S. Liu, Q. Wang, H. Xiao, K. Wang, C. Wang, X. Wang, W. Ge, Z. Wang, Optimization of growth and fabrication techniques to enhance the InGaN/GaN multiple quantum well solar cells performance, Superlattices Microstruct. 109 (2017) 194–200, https://doi.org/10.1016/j.spmi.2017.05.014.
[105] L. Sang, M. Sumiya, M. Liao, Y. Koide, X. Yang, B. Shen, Polarization-induced hole doping for long-wavelength In-rich InGaN solar cells, Appl. Phys. Lett. 119 (2021), 202103, https://doi.org/10.1063/5.0071506.
[106] J. Bai, Y.P. Gong, Z. Li, Y. Zhang, T. Wang, Semi-polar InGaN/GaN multiple quantum well solar cells with spectral response at up to 560 nm, Sol. Energy Mater. Sol. Cells 175 (2018) 47–51, https://doi.org/10.1016/j.solmat.2017.10.005.
[107] X.M. Cai, X.Q. Lv, X.J. Huang, X.L. Wang, M.S. Wang, L. Yang, H.L. Zhu, B.P. Zhang, Study of InGaN/GaN multiple quantum well solar cells with different barrier thicknesses, Phys. Status Solidi A 215 (2018), 1700581, https://doi.org/10.1002/pssa.201700581.
[108] C.A. M Fabien, A. Maros, C.B. Honsberg, W.A. Doolittle, III-Nitride double-heterojunction solar cells with high In-content InGaN absorbing layers: comparison of large-area and small-area devices, IEEE J. Photovoltaics 6 (2016) 460–464, https://doi.org/10.1109/JPHOTOV.2015.2504790.
[109] K. Wang, D. Imai, K. Kusakabe, A. Yoshikawa, Leak path passivation by in situ Al-N for InGaN solar cells operating at wavelengths up to 570 nm, Appl. Phys. Lett. 108 (2016), 092105, https://doi.org/10.1063/1.4942507.
[110] Y.K. Lee, M.H. Lee, C. M Cheng, C.H. Yang, Enhanced conversion efficiency of InGaN multiple quantum well solar cells grown on a patterned sapphire substrate, Appl. Phys. Lett. 98 (2011), 263504, https://doi.org/10.1063/1.3605244.
[111] Y.S. Kwak, D.S. Lee, K.H. Kim, W.H. Kim, S.W. Moon, Growth and characterization of AlGaN films on patterned sapphire substrates, AIP Conf. Proc. 1399 (2011) 179, https://doi.org/10.1063/1.3666314.
[112] N.G. Young, R.M. Farrell, Y.L. Hu, Y. Terao, M. Iza, S. Keller, S.P. DenBaars, S. Nakamura, J.S. Speck, High performance thin quantum barrier InGaN/GaN solar cells on sapphire and bulk (0001) GaN substrates, Appl. Phys. Lett. 103 (2013), 173903, https://doi.org/10.1063/1.4826483.
[113] W.A. Melton, J.I. Pankove, GaN growth on sapphire, J. Cryst. Growth 178 (1997) 168–173, https://doi.org/10.1016/S0022-0248(97)00082-1.
[114] X.J. Ning, F.R. Chien, P. Pirouz, J.W. Yang, M.A. Khan, Growth defects in GaN films on sapphire: the probable origin of threading dislocations, J. Mater. Res. 11 (1996) 580–592, https://doi.org/10.1557/JMR.1996.0071.
[115] S. Nakamura, GaN growth using GaN buffer layer, Jpn. J. Appl. Phys. 30 (1991) L1705, https://doi.org/10.1143/JJAP.30.L1705.
[116] R.C. White, M. Khoury, F. Wu, S. Keller, M. Rozhavskaia, D. Shotta, S. Nakaruma, S.P. DenBaars, MOCVD growth of thick V-pit-free InGaN films on semi-relaxed InGaN substrates, Semicond. Sci. Technol. 36 (2021), 015011, https://doi.org/10.1088/1361-6641/abc51c.
[117] A. Even, G. Laval, O. Ledoux, P. Ferret, P. Ferret, D. Shotta, E. Guiot, F. Levy, I.C. Robin, A. Dussaigne, Enhanced in incorporation in full InGaN heterostructure grown on relaxed InGaN pseudo-substrate, Appl. Phys. Lett. 110 (2017), 262103, https://doi.org/10.1063/1.4989998.
[118] K. Hestroffer, F. Wu, H. Li, C. Lund, S. Keller, J.S. Speck, U.K. Mishra, Relaxed c-plane InGaN layers for the growth of strain-reduced InGaN quantum wells, Semicond. Sci. Technol. 30 (2015), 105015, https://doi.org/10.1088/0268-1242/30/10/105015.
[119] B.-T. Tran, et al., Fabrication and characterization of n-$In_{0.4}Ga_{0.6}N$/p-Si solar cell, Sol. Energy Mater. Sol. Cells 102 (2012) 208–211, https://doi.org/10.1016/j.solmat.2012.03.030.
[120] P. Aseev, et al., Uniform low-to-high in composition InGaN layers grown on Si, Appl. Phys. Express 6 (2013), 115503, https://doi.org/10.7567/APEX.6.115503.
[121] P. Prajon, D. Nirmal, M.A. Menokey, J.C. Pravin, Efficiency enhancement of InGaN MQW LED using compositionally step graded InGaN barrier on SiC substrate, J. Disp. Technol. 12 (2016) 1117–1121, https://doi.org/10.1109/JDT.2016.2570814.
[122] K. Wang, Q. Wang, J. Chu, H. Xiao, X. Wang, Z. Wang, Roles of polarization effects in InGaN/GaN solar cells and comparison of p-i-n and n-i-p structures, Opt Express 26 (2018) 946–954, https://doi.org/10.1364/OE.26.00A946.
[123] E.T. Yu, X.Z. Dang, P.M. Asbeck, S.S. Lau, G.J. Sullivan, Spontaneous and piezoelectric polarization effects in III–V nitride heterostructures, J. Vac. Sci. Technol. B 17 (1999) 1742, https://doi.org/10.1116/1.590818.

[124] C.J. Neufeld, et al., Effect of doping and polarization on carrier collection in InGaN quantum well solar cells, Appl. Phys. Lett. 98 (2011), 243507, https://doi.org/10.1063/1.3595487.
[125] O. Ambacher, et al., Role of spontaneous and piezoelectric polarization induced effects in group-III nitride based heterostructures and devices, Phys. Status Solidi B 216 (1999) 381–389, https://doi.org/10.1002/(SICI)1521-3951(199911)216:1%3C381::AID-PSSB381%3E3.0.CO;2-O.
[126] K. Wang, Q. Wang, J. Chu, H. Xiao, X. Wang, Z. Wang, Roles of polarization effects in InGaN/GaN solar cells and comparison of p-i-n and n-i-p structures, Opt Express 26 (2018) A946–A954, https://doi.org/10.1364/OE.26.00A946.
[127] S. Inoue, M. Katoh, A. Kobayashi, J. Ohta, H. Fujioka, Investigation on the conversion efficiency of InGaN solar cells fabricated on GaN and ZnO substrates, Phys. Status Solidi Rapid Res. Lett. 4 (2010) 88–90, https://doi.org/10.1002/pssr.201004044.
[128] J.R. Dickerson, K. Pantzas, A. Ougazzaden, P.L. Voss, Polarization-induced electric fields make robust n-GaN/i-InGaN/p-GaN solar cells, IEEE Electron. Device Lett. 34 (2013) 363–365, https://doi.org/10.1109/LED.2012.2237376.
[129] X. Cai, S. Zeng, B. Zhang, Fabrication and characterization of InGaN p-i-n homojunction solar cell, Appl. Phys. Lett. 95 (2009), 173504, https://doi.org/10.1063/1.3254215.
[130] M. Sarollahi, M. Zamani-Alavijeh, R. Allaparthi, M.A. Aldawsari, M. Refaei, R. Alhelais, M.H.U. Maruf, Y.I. Mazur, M.E. Ware, Ware Study of simulations of double graded InGaN solar cell structures, J. Vac. Sci. Technol. B 40 (2022), 042203, https://doi.org/10.1116/6.0001841.
[131] J.R. Lang, N.G. Young, R.M. Farrell, Y.R. Wu, J.S. Speck, Carrier escape mechanism dependence on barrier thickness and temperature in InGaN quantum well solar cells, Appl. Phys. Lett. 101 (2012), 181105, https://doi.org/10.1063/1.4765068.
[132] H.C. Lee, Y.K. Su, W.K. Chuang, J.C. Lin, K.C. Huang, Y.C. Cheng, K.J. Chang, Discussion on electrical characteristics of i-$In_{0.13}Ga_{0.87}N$ p-i-n photovoltaics by using a single/multi-antireflection layer, Sol. Energy Mater. Sol. Cells 94 (2010) 1259–1262, https://doi.org/10.1016/j.solmat.2010.03.020.
[133] N.G. Young, E.E. Perl, R.M. Farrell, M. Iza, S. Keller, J.E. Bowers, S. Nakamura, S.P. DenBaars, J.S. Speck, High-performance broadband optical coatings on InGaN/GaN solar cells for multijunction device integration, Appl. Phys. Lett. 104 (2014), 163902, https://doi.org/10.1063/1.4873117.
[134] G.J. Lin, K.Y. Lai, C.A. Lin, Y.L. Lai, J.H. He, Efficiency enhancement of InGaN-based multiple quantum well solar cells employing antireflective ZnO nanorod arrays, IEEE Electron. Device Lett. 32 (2011) 1104–1106, https://doi.org/10.1109/LED.2011.2158061.
[135] D.-J. Seo, J.-P. Shim, S.-B. Choi, T.H. Seo, E.-K. Suh, D.-S. Lee, Efficiency improvement in InGaN-based solar cells by indium tin oxide nano dots covered with ITO films, Opt Express 20 (2012) 991–996, https://doi.org/10.1364/OE.20.00A991.
[136] J. Bai, C.C. Yang, M. Athanasiou, T. Wang, Efficiency enhancement of InGaN/GaN solar cells with nanostructures, Appl. Phys. Lett. 104 (2014), 051129, https://doi.org/10.1063/1.4864640.
[137] J. Bai, M. Athanasiou, T. Wang, Influence of the ITO current spreading layer on efficiencies of InGaN-based solar cells, Sol. Energy Mater. Sol. Cells 145 (2016) 226–230, https://doi.org/10.1016/j.solmat.2015.10.026.
[138] S. Yamamoto, et al., Properties of nitride-based photovoltaic cells under concentrated light illumination, Phys. Status Solidi Rapid Res. Lett. 6 (2012) 145–147, https://doi.org/10.1002/pssr.201206038.
[139] J.-K. Sheu, F.-B. Chen, S.-H. Wu, M.-L. Lee, P.-C. Chen, Y.-H. Yeh, Vertical InGaN-based green-band solar cells operating under high solar concentration up to 300 suns, Opt. Express 22 (2014) 1222–1228, https://doi.org/10.1364/OE.22.0A1222.
[140] M. Mori, S. Kondo, S. Yamamoto, T. Nakao, M. Iwaya, T. Takeuchi, S. Kamiyama, I. Akasaki, H. Amano, Concentrating properties of nitride-based solar cells using different electrodes, Jpn. J. Appl. Phys. 52 (2013), 08JH02, https://doi.org/10.7567/JJAP.52.08JH02.
[141] J.J. Williams, et al., Development of a high-band gap high temperature III-nitride solar cell for integration with concentrated solar power technology, in: 2017 IEEE 44th Photovoltaic Specialist Conference (PVSC), Washington D.C., United States, 2017, pp. 193–195, https://doi.org/10.1109/PVSC.2016.7749576.
[142] A. Caria, et al., Degradation and recovery of high-periodicity InGaN/GaN MQWs under optical stress in short-circuit condition, Proc. SPIEL (2020) 112800E, https://doi.org/10.1117/12.2547590, 11280 (San Francisco, United States.
[143] G. Moses, X. Huang, Y. Zhao, M.A.d. Maur, E.A. Katz, J.M. Gordon, InGaN/GaN multi-quantum-well solar cells under high solar concentration and elevated temperatures for hybrid solar thermal-photovoltaic power plants, Prog. Photovoltaics Res. Appl. 28 (2020) 1167–1174, https://doi.org/10.1002/pip.3326.
[144] Y.H. Cho, G.H. Gainer, A.J. Fischer, J.J. Song, S. Keller, U.K. Mishra, S.P. DenBaars, "S-shaped" temperature-dependent emission shift and carrier dynamics in InGaN/GaN multiple quantum wells, Appl. Phys. Lett. 73 (1998) 1370–1372, https://doi.org/10.1063/1.122164.
[145] T.J. Badcock, R. Hao, M.A. Moram, M.J. Kappers, P. Dawson, R.A. Oliver, C.J. Humphreys, Recombination mechanisms in heteroepitaxial non-polar InGaN/GaN quantum wells, J. Appl. Phys. 112 (2012), 013534, https://doi.org/10.1063/1.4731730.
[146] S. Marcinkevičius, K.M. Kelchner, L.Y. Kuritzky, S. Nakamura, S.P. DenBaars, J.S. Speck, Photoexcited carrier recombination in wide m-plane InGaN/GaN quantum wells, Appl. Phys. Lett. 103 (2013), 111107, https://doi.org/10.1063/1.4820839.
[147] M. Shahmohammadi, et al., Enhancement of Auger recombination induced by carrier localization in InGaN/GaN quantum wells, Phys. Rev. B 95 (2017), 125314, https://doi.org/10.1103/PhysRevB.95.125314.
[148] I. Vurgaftman, J.R. Meyer, Band parameters for nitrogen-containing semiconductors, J. Appl. Phys. 94 (2003) 3675–3696, https://doi.org/10.1063/1.1600519.
[149] S.T. Liu, et al., Temperature-controlled epitaxy of $In_xGa_{1-x}N$ alloys and their band gap bowing, J. Appl. Phys. 110 (2011), 113514, https://doi.org/10.1063/1.3668111.
[150] B. Sheng, et al., Intensive luminescence from a thick, indium-rich $In_{0.7}Ga_{0.3}N$ film, Jpn. J. Appl. Phys. 58 (2019), 065503, https://doi.org/10.7567/1347-4065/ab1a5b.
[151] P. Li, et al., Demonstration of ultra-small $5 \times 5\ \mu m^2$ 607 nm InGaN amber micro-light-emitting diodes with an external quantum efficiency over 2%, Appl. Phys. Lett. 120 (2022), 041102 https://doi.org/10.1063/5.0078771.
[152] Z. Zhuang, D. Iida, P. Kirilenko, K. Ohkawa, Improved performance of InGaN-based red light-emitting diodes by micro-hole arrays, Opt Express 29 (2021) 29780–29788, https://doi.org/10.1364/OE.435556.